



**HAL**  
open science

## **Cyclophilin A allows the allosteric regulation of a structural motif in the disordered domain 2 of NS5A and thereby fine-tunes HCV RNA replication**

Marie Dujardin, Vanesa Madan, Neha S Gandhi, François-Xavier Cantrelle, Hélène Launay, Isabelle Huvent, Ralf Bartenschlager, Guy Lippens, Xavier Hanouille

### ► To cite this version:

Marie Dujardin, Vanesa Madan, Neha S Gandhi, François-Xavier Cantrelle, Hélène Launay, et al.. Cyclophilin A allows the allosteric regulation of a structural motif in the disordered domain 2 of NS5A and thereby fine-tunes HCV RNA replication. *Journal of Biological Chemistry*, 2019, 294 (35), pp.13171-13185. 10.1074/jbc.RA119.009537. hal-02998113

**HAL Id: hal-02998113**

**<https://hal.science/hal-02998113>**

Submitted on 10 Nov 2020

**HAL** is a multi-disciplinary open access archive for the deposit and dissemination of scientific research documents, whether they are published or not. The documents may come from teaching and research institutions in France or abroad, or from public or private research centers.

L'archive ouverte pluridisciplinaire **HAL**, est destinée au dépôt et à la diffusion de documents scientifiques de niveau recherche, publiés ou non, émanant des établissements d'enseignement et de recherche français ou étrangers, des laboratoires publics ou privés.



# Cyclophilin A allows the allosteric regulation of a structural motif in the disordered domain 2 of NS5A and thereby fine-tunes HCV RNA replication

Received for publication, May 27, 2019, and in revised form, June 28, 2019. Published, Papers in Press, July 17, 2019, DOI 10.1074/jbc.RA119.009537

Marie Dujardin<sup>‡1</sup>, Vanesa Madan<sup>§2,3</sup>, Neha S. Gandhi<sup>¶2</sup>, François-Xavier Cantrelle<sup>‡</sup>, H el ene Launay<sup>‡4</sup>, Isabelle Huvent<sup>‡</sup>, Ralf Bartenschlager<sup>§</sup>,  Guy Lippens<sup>‡5</sup>, and  Xavier Hanouille<sup>‡6</sup>

From the <sup>‡</sup>University of Lille, CNRS, UMR 8576, UGSF-Unit e de Glycobiologie Structurale et Fonctionnelle, F-59000 Lille, France, the <sup>§</sup>Department of Infectious Diseases, Molecular Virology, University of Heidelberg, 69120 Heidelberg, Germany, and the <sup>¶</sup>School of Mathematical Sciences and Institute for Health and Biomedical Innovation, Queensland University of Technology, Brisbane, Queensland 4000, Australia

Edited by Charles E. Samuel

Implicated in numerous human diseases, intrinsically disordered proteins (IDPs) are dynamic ensembles of interconverting conformers that often contain many proline residues. Whether and how proline conformation regulates the functional aspects of IDPs remains an open question, however. Here, we studied the disordered domain 2 of nonstructural protein 5A (NS5A-D2) of hepatitis C virus (HCV). NS5A-D2 comprises a short structural motif (PW-turn) embedded in a proline-rich sequence, whose interaction with the human prolyl isomerase cyclophilin A (CypA) is essential for viral RNA replication. Using NMR, we show here that the PW-turn motif exists in a conformational equilibrium between folded and disordered states. We found that the fraction of conformers in the NS5A-D2 ensemble that adopt the structured motif is allosterically modulated both by the *cis/trans* isomerization of the surrounding prolines that are CypA substrates and by substitutions conferring resistance to cyclophilin inhibitor. Moreover, we noted that this fraction is directly correlated with HCV RNA replication efficiency. We conclude that CypA can fine-tune the

dynamic ensemble of the disordered NS5A-D2, thereby regulating viral RNA replication efficiency.

Hepatitis C virus (HCV)<sup>7</sup> is a positive sense single-stranded RNA (~9.6 kb) virus, belonging to the *Flaviviridae* family. It is estimated that worldwide ~71 million people have a chronic HCV infection ([www.who.int/mediacentre/factsheets/fs164/en/](http://www.who.int/mediacentre/factsheets/fs164/en/)). This can lead to progressive hepatic injuries, such as cirrhosis or even hepatocellular carcinoma (2). Each year, chronic hepatitis C is responsible for the death of roughly 400,000 people with ~25% of all liver cancer cases being linked to HCV infection.

The HCV genome has one large ORF, encoding a polyprotein precursor that is proteolytically processed into 10 mature proteins by both host and viral proteases. The structural proteins (core, E1 and E2) constitute the viral particle, and the nonstructural (NS) proteins (p7, NS2, NS3, NS4A, NS4B, NS5A, and NS5B) are involved in virion formation and RNA replication (3, 4). NS3 to NS5B, bound to double-membrane vesicles (DMV) derived from the host endoplasmic reticulum (ER), constitute the viral replication machinery (5–7). This complex, by means of the RNA-dependent RNA polymerase activity of NS5B, replicates the viral genome (8, 9).

NS5A is a key multifunctional phosphoprotein (49 kDa) that is essential for HCV genome replication (10, 11) and is also involved in virion production (12). NS5A is known to interact with numerous viral and host proteins (4, 13–15). NS5A, which

This work was supported by French National Agency for Research (ANR) Grant ANR-11-JSV8-005 and French National Agency for Research on AIDS and Viral Hepatitis (ANRS) Grant A02014-2, a fellowship from Lille University (to M. D.), Deutsche Forschungsgemeinschaft (German Research Foundation) Project Grant 112927078-TRR 83 (to V. M. and R. B.), and by Research Federation "structural and functional biochemistry of BIOMolecular Assemblies" (CNRS, FR-3688). The authors declare that they have no conflicts of interest with the contents of this article.

This article contains Table S1, Figs. S1–S21, and supporting information.

The NMR data reported in this paper has been submitted to the Biological Magnetic Resonance Data Bank under accession number 30037.

The atomic coordinates and structure factors (code 6HT4) have been deposited in the Protein Data Bank (<http://www.pdb.org/>).

<sup>1</sup> Present address: University of Lyon, CNRS, UMR 5086, MMSB, Molecular Microbiology and Structural Biochemistry, F-69367 Lyon, France.

<sup>2</sup> Both authors contributed equally to this work.

<sup>3</sup> Present address: MRC Laboratory of Molecular Biology, Francis Crick Ave., CB2 0QH, Cambridge, UK.

<sup>4</sup> Present address: University of Aix-Marseille, CNRS, UMR 7281, BIP, Bio energetique et Ing enierie des Prot eines, F-13402 Marseille, France.

<sup>5</sup> Present address: Laboratoire d'Ing enierie des Syst emes Biologiques et des Proc ed es, INSA, University of Toulouse, CNRS, INRA, F-31077 Toulouse, France.

<sup>6</sup> To whom correspondence should be addressed: Univ. Lille, CNRS, UMR 8576, UGSF, Unit e de Glycobiologie Structurale et Fonctionnelle, Campus CNRS de la Haute-Borne, 50 Avenue du Halley, 59000 Lille, France. Tel.: 33-0-362-531-716; E-mail: [xavier.hanouille@univ-lille.fr](mailto:xavier.hanouille@univ-lille.fr).

<sup>7</sup> The abbreviations used are: HCV, hepatitis C virus; CA, capsid protein; CHESPA, chemical shift projection analysis; CypA, cyclophilin A; CypIs, cyclophilin inhibitors; CsA, cyclosporin A; dPCA, dihedral principal component analysis; DAAs, direct-acting antivirals; DMV, double-membrane vesicles; ER, endoplasmic reticulum; GaMD, gaussian accelerated molecular dynamics; HTAs, host-targeted antivirals; HSQC, heteronuclear single quantum correlation; IDPs/IDRs, intrinsically disordered proteins (or regions); MD, molecular dynamics; NS, non-structural proteins; NS5A, non-structural protein 5A; NS5A-D1, domain 1 of NS5A; NS5A-D2, domain 2 of NS5A; NS5A-D3, domain 3 of NS5A; PepD2-WT, peptide corresponding to residues 304–323 of NS5A-D2; PPIase, peptidyl-prolyl *cis/trans* isomerase; PTMs, post-translational modifications; PW\_fraction, fraction of the conformers that hold the structured PW-turn motif; PW-turn, short structural motif in NS5A-D2; TMSP, sodium 3-trimethylsilyl-[2,2,3,3-d<sub>4</sub>]propionate; r.m.s., root mean square; RDC, residual dipolar coupling; dPCA, dihedral principal component analysis.

## Conformational regulation of NS5A-D2 by CypA

is bound to the ER membrane via an N-terminal amphipathic helix (16), is composed by a folded cytoplasmic domain (NS5A-D1) (11) and two intrinsically disordered domains (NS5A-D2 and -D3) (17–19) (Fig. 1a). No enzymatic activity has been identified for any of these domains. Different homodimeric structures of NS5A-D1 (11, 20, 21) suggested it might be implicated in RNA-binding (22). Importantly, this domain is the molecular target for direct-acting antivirals (DAAs) against NS5A (23, 24). NS5A-D2 and -D3 are intrinsically disordered, and thus exist as a dynamic ensemble of conformers. NS5A-D2 is required for viral RNA replication (10), whereas NS5A-D3 is involved in viral particle production and assembly (12). We and others have shown that NS5A-D2 and -D3 interact with and are substrates of human cyclophilin A (CypA) (25–27), a peptidyl-prolyl *cis/trans* isomerase (PPIase) that is an essential host factor for HCV replication (28). Detailed analysis assigned the main CypA-binding site to a small region (about 20 amino acid residues) in NS5A-D2 that contains 5 strictly conserved residues across the seven HCV genotypes, among which are 3 proline residues (25, 29). An even shorter peculiar structural motif, called PW-turn (<sup>314</sup>PXWA<sup>317</sup> in the Con1 strain, genotype 1b), which is essential for HCV RNA replication was identified in this region (30) (Fig. 1a). Disruption of the PW-turn weakens the molecular interaction between NS5A-D2 and CypA, but is required for efficient prolyl *cis/trans* isomerase activity of CypA toward the <sup>313</sup>Met–Pro<sup>314</sup> bond, contrary to the other prolyl bonds of the domain (30). The interaction between NS5A-D2 and CypA can be inhibited by cyclosporin A (CsA) or its non-immunosuppressive analogs such as alisporivir, SCY-635, or NIM-811, or by other small-molecule cyclophilin inhibitors (31–34). These compounds thereby act as host-targeted antivirals (HTAs). NS5A hence can be equally targeted by DAAs (via NS5A-D1) or HTAs (via NS5A-D2 through its interaction with CypA). Of note, studies of HCV NS5A and CypA paved the way for the use of CypI for other viral infections such as human coronaviruses (e.g. MERS or SARS) that also require CypA for their replication (35).

The role(s) of CypA in HCV replication and the mechanism of action of cyclophilin inhibitors (CypIs) are complex and still not completely understood. CypIs bind host CypA in a single hydrophobic pocket that contains both its enzymatic PPIase and binding activities, and thereby disrupt both the molecular interaction between CypA and NS5A-D2 as well as the putative CypA PPIase activity toward selected prolyl bonds in NS5A-D2 (25, 36, 37). Therefore, all CypA catalytic mutants are also impaired in their binding properties. Several laboratories have demonstrated that CypIs inhibit the *de novo* formation of the DMVs, the HCV-induced membrane structures that hold the replication complex (38, 39). A remodeling of the ER in the presence of CypIs has also been observed in HCV-infected cells (40). Most of the identified CypI-resistance mutations, such as D320E, D320E,Y321N, and Y321H (28, 41, 42), are located in the immediate proximity of the PW-turn in NS5A-D2. These mutations confer a moderate resistance (~2–4-fold) to CypIs and hence a partial CypA independence, but do not abolish the interaction between CypA and NS5A-D2 (27, 43, 44). A better understanding of the functional role(s) of both CypA and NS5A, and specifically of the disordered domains of the latter,

in the HCV life cycle could shed light on the underlying molecular mechanisms of this resistance.

Intrinsically disordered proteins (or regions) (IDPs/IDRs) are functional despite not having a stable 3D structure (45, 46). They are best described as dynamic ensembles of interconverting conformers. Their biological functions are usually related to their capacity to interact with numerous partners, with a high specificity often related to low affinity (even if subnanomolar affinities have been reported (47)). As a consequence, they are often described as molecular hubs. IDPs/IDRs, despite any enzymatic activity, are nonetheless involved in cell signaling and regulatory processes, which can be physiological or pathological. Indeed, their implication has been demonstrated in numerous human diseases, including cancer, neurodegeneration, diabetes, and viral infections (48). IDPs/IDRs can interact with a biological partner while remaining disordered and form fuzzy complexes (49), but they can also establish interactions using short peptide motifs, including short linear motifs (50), molecular recognition features (51), or pre-structured motifs (52), and then fold upon binding. The biological functions of IDPs/IDRs are further regulated by alternative splicing and post-translational modifications (PTMs), including phosphorylation, ubiquitination, and glycosylation (53). These PTMs can modulate the structural and conformational properties of IDPs/IDRs and thereby break or promote interactions. IDPs are also enriched in proline residues (54), but whether these have any functional role has not yet been described in a conclusive manner. More recently, the concept of allostery has been expanded from its original paradigm (55) and allosteric regulations have been described in disordered protein (56, 57). It has been shown that allosteric perturbations (ligand binding, PTMs, mutations) can change the functional properties of IDPs/IDRS by remodeling their energy landscape or conformational ensemble (*i.e.* population shift). This extreme complexity allows IDPs/IDRs to exert a fine modulation of biological processes (58).

Here, we combine nuclear magnetic resonance (NMR) spectroscopy with molecular dynamics (MD) simulations to decipher the role of the proline residues on the structural disorder in HCV NS5A-D2, and link it to its functional consequences. The detailed conformational behavior of NS5A-D2 (JFH1 strain, genotype 2a) with its PW-turn structural motif centered on <sup>310</sup>PAWA<sup>313</sup> confirms its pan-genotypic importance for HCV. Using the Trp<sup>312</sup> resonance as a probe, we show that the NS5A-D2 region encompassing the PW-turn exhibits a peculiar dynamic behavior whereby it may adopt, at least 2 conformational states, one structured with the PW-turn conformation fully formed and one totally disordered. These two states are in the fast-exchange NMR regime. Unexpectedly, we find that the *cis/trans* isomerization state of the 5 surrounding proline residues affects the ratio of conformers that adopt or not the PW-turn motif in the NS5A-D2 ensemble. Hence, this structural motif is allosterically regulated by proline *cis/trans* equilibria. CypA, through catalyzing the interconversion for distinct prolines, can thereby connect these different ensembles on a subsecond time scale. Importantly, we find that the CypI-resistance mutations in NS5A-D2 correspond to similar allosteric perturbations as they favor ensembles with a

decreased structured PW-turn population. Using a cell-based assay, we show that the population of the structured PW-turn motif in the ensemble directly correlates with HCV RNA replication efficiency. Our results reveal a complex mechanism in which CypA modulates NS5A-D2's function.

## Results

### NMR characterization of NS5A-D2 and its PW-turn motif

The  $^1\text{H}$ ,  $^{15}\text{N}$ -HSQC NMR spectrum of NS5A-D2 of the HCV JFH1 strain (genotype 2a) (Fig. 1*b*) displays a narrow  $^1\text{H}$  chemical shift dispersion that confirms the high level of intrinsic disorder in this domain (Fig. S1*a*) (18). The secondary structure propensity analysis, based on the  $^{13}\text{C}$  chemical shifts, indicates the presence of several residual  $\alpha$ -helices and extended regions in the N-terminal half (Fig. 1*c*). This is similar to the observations made on NS5A-D2 from HCV strains HC-J4 and Con1 (both genotype 1b) (30, 59). Comparison of the experimental  $^1\text{H}$  and  $^{15}\text{N}$  chemical shifts of NS5A-D2 (JFH1) with those predicted for a truly disordered protein (60) highlights unexpected values for the tryptophan 312 (Trp<sup>312</sup>) residue in the C-terminal part of the domain (Fig. 1*d* and Figs. S1 and S2). A similar observation was made for the equivalent Trp<sup>316</sup> residue in NS5A-D2 of the HCV Con1 strain and was attributed to the presence of the PW-turn structural motif in the most conserved region of NS5A-D2 (30). The primary sequence of the PW-turn in the Con1 strain is  $^{314}\text{PIWA}^{317}$ , whereas it is  $^{310}\text{PAWA}^{313}$  in JFH1. In this motif, all positions but the second are strictly conserved in all HCV genotypes. We used a 20-mer peptide (pepD2-WT) to obtain an atomic description of this region in NS5A-D2 (JFH1) (Fig. S3). All the NMR data ( $^1\text{H}$ ,  $^{15}\text{N}$ ,  $^{13}\text{C}$  chemical shifts, NOE contacts, as well  $^3J_{\text{HN-H}\alpha}$  couplings) were used to calculate a NMR structural model of this PW-turn (Fig. 2 and Fig. S4*a*). The local r.m.s. deviation values suggest that beyond the core of the PW-turn (*i.e.*  $^{310}\text{PAWA}^{313}$ ), where the ring of Pro<sup>310</sup> and the aromatic side chain of Trp<sup>312</sup> are engaged in a CH/ $\pi$  interaction (61), the residues at its C terminus also adopt a certain degree of order (Fig. 2*b*). The interaction of the PW-turn motif, and specifically the Trp<sup>312</sup> residue, with the Tyr<sup>317</sup> side chain and the rings of Pro<sup>319</sup> and Pro<sup>320</sup> (Fig. 2*c*) agree with a similar extension of the motif as described in the peptide when bound to the MOBKL1B protein (62). Conformations of pepD2-WT, free in solution (this study), are closely related to its structure in the crystallographic complex with MOBKL1B (Fig. S4*b*).

The plot of the  $^1\text{H}$ ,  $^{15}\text{N}$ -HSQC peak intensity along the NS5A-D2 sequence reveals that the resonances in the N-terminal moiety are narrower than those in the C-terminal half (Fig. 1*e*).  $^{15}\text{N}$  spin relaxation data on the full-length domain confirmed this, with higher  $R^2$  values for the 304–321 region of NS5A-D2. Heteronuclear NOE values in this region are also clearly positive, whereas they are negative or close to zero for most residues in the N-terminal half of the fragment. We hence conclude that this region, encompassing the PW-turn and corresponding to the host CypA-binding site (25), is characterized by an increased rigidity while simultaneously experiencing exchange broadening (63) (Fig. 1, *f–h*). We next measured the residual dipolar couplings ( $\text{RDC}_{\text{NH}}$ ) of the individual HN vec-

tors in NS5A-D2 using a partially oriented sample (Fig. 1*i*). The residues in the region 304–321 display  $\text{RDC}_{\text{NH}}$  values higher than expected for an IDR (64). The highest value (32.8 Hz) was observed for the Trp<sup>312</sup> residue in the PW-turn motif. The  $\text{RDC}_{\text{NH}}$  values from the Trp<sup>312</sup> and Trp<sup>325</sup> side chains were 40 and 24 Hz, respectively (data not shown). Altogether, these data confirm that the CypA-binding site contains a structured PW-turn motif with nevertheless a peculiar structural dynamics.

We have previously reported that the I315G mutation in a peptide derived from NS5A-D2 of the Con1 strain precludes the presence of the PW-turn motif without making any change on the conserved residues. To investigate the functional role of the PW-turn motif in the JFH1 strain, we introduced the analogous mutation, A311G, in NS5A-D2. We found that this mutation also efficiently disrupts the PW-turn in NS5A-D2 because in the different NMR spectra acquired on this NS5A-D2 mutant, the proton amide and  $^{13}\text{C}\alpha$  resonances of Trp<sup>312</sup> and Ala<sup>313</sup> move toward their expected frequencies for a fully disordered region (Figs. S1*b* and S5). The NS5A-D2 A311G mutant hence provides a way to assess the structural and functional role(s) played by the PW-turn motif in the CypA-binding site.

### Proline conformations induced a linear chemical shift pattern for Trp<sup>312</sup>

Upon closer examination of the  $^1\text{H}$ ,  $^{15}\text{N}$ -HSQC of NS5A-D2 WT, we identified up to six resonances that could be assigned to the same Trp<sup>312</sup> residue (Fig. 3*a*). Based on the peak intensity, there are one major (W312\_1) and five minor (W312\_2 to W312\_6) Trp<sup>312</sup> resonances. As the Trp<sup>312</sup> residue is surrounded by 5 different proline residues in NS5A-D2, we hypothesized that this conformational heterogeneity with slow exchange on the time scale imposed by the chemical shift differences between the individual resonances could correspond to the *cis/trans* equilibria of these individual proline residues. Evidence was found in the  $^1\text{H}$ ,  $^{15}\text{N}$ ,  $^{13}\text{C}$  3D experiments used for the assignment of the fragment. Starting from the proton amide W312\_6 resonance and using the  $^{13}\text{C}$  chemical shifts ( $C\alpha$ ,  $C\beta$ , and CO), we connected it, in a sequential fashion, to a minor resonance of the Ala<sup>311</sup> residue (A311\_6), which is itself linked to a residue with  $^{13}\text{C}$  chemical shifts typical of a *cis*-proline (62.4 and 34.3 ppm for  $C\alpha$  and  $C\beta$ , respectively) (65) (Fig. S6). Thus, the minor W312\_6 resonance originates from the *cis* conformation of the Pro<sup>310</sup> residue. Likewise, the other minor Trp<sup>312</sup> resonances are also related to the *cis* conformation of proline residues. Indeed, in a  $^1\text{H}$ ,  $^{15}\text{N}$ -heteronuclear *zz*-exchange experiment (66) in the presence of a catalytic amount of CypA, we identified exchange cross-peaks connecting each of the minor Trp<sup>312</sup> resonances (W312\_2 to W312\_6) to the major one (W312\_1) (Fig. 3*b*). To link each of the minor Trp<sup>312</sup> resonances to a particular proline residue, we compared the  $^1\text{H}$ ,  $^{15}\text{N}$ -HSQC spectra of NS5A-D2 Pro to Ala mutants (NS5A-D2 P306A, P310A, P315A, P319A, and P320A) with that of the WT construct (Figs. S7–S11) (67). In each mutant spectrum, a minor Trp<sup>312</sup> resonance is missing. We therefore could unambiguously assign the minor Trp<sup>312</sup> resonances in the  $^1\text{H}$ ,  $^{15}\text{N}$ -HSQC of NS5A-D2 WT to subpopulations of the peptide with a single prolyl bond in the *cis* conformation (Fig.

## Conformational regulation of NS5A-D2 by CypA

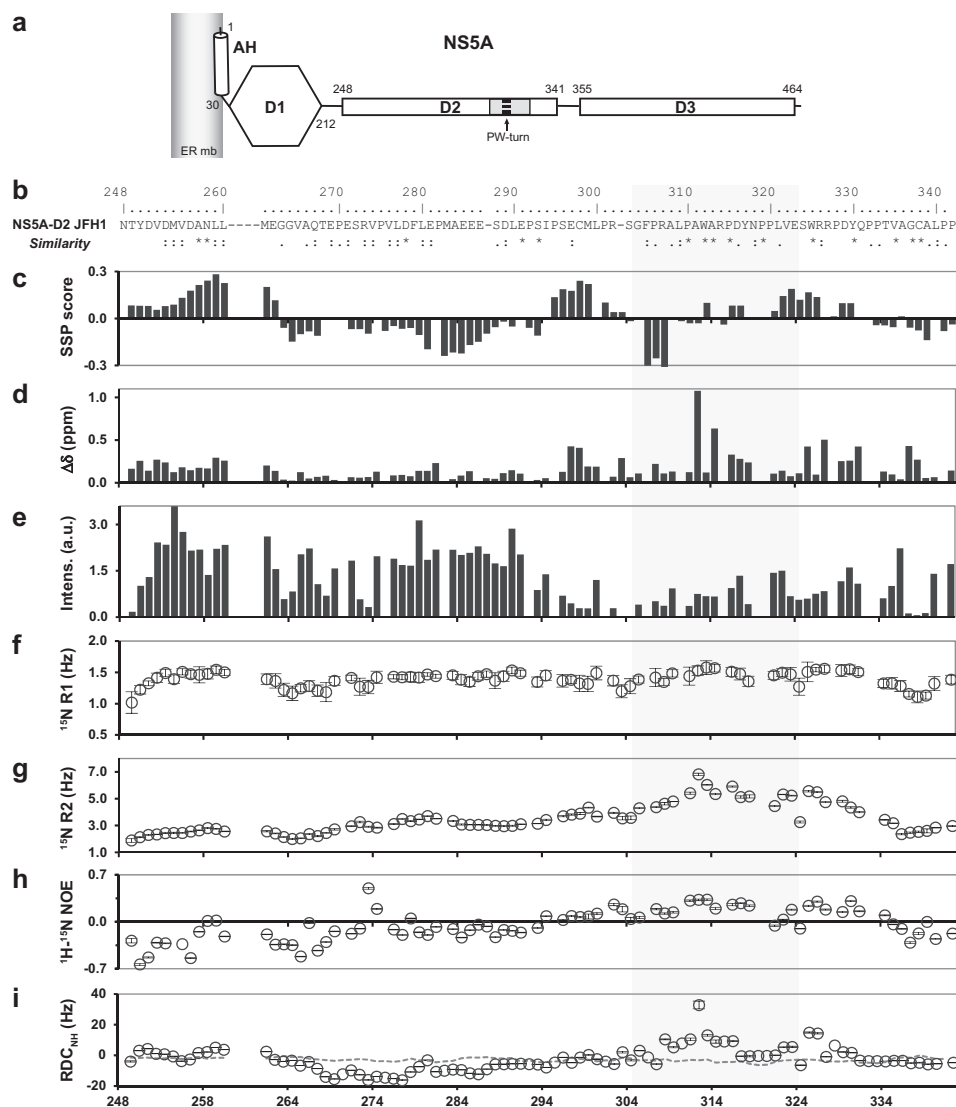


**Figure 1. NMR structural dynamics of NS5A-D2.** *a*, schematic representation of HCV NS5A protein anchored to the cytoplasmic side of the ER membrane via a N-terminal amphipathic helix (AH). Its folded domain 1 (NS5A-D1) is shown as a white hexagon, whereas its disordered domains 2 and 3 (NS5A-D2 and -D3) are represented by white rectangles. The CypA-binding site, which comprises the PW-turn motif (dashed black line), is shown as a gray area. *b*, NS5A-D2 amino acid sequence (residue 248–342) from HCV JFH1 strain (genotype 2a). Below is similarity deduced from the alignment of reference sequences from all confirmed HCV genotypes and subtypes. The light gray shaded region corresponds to the PepD2-WT peptide, which is also the CypA-binding site. *c*, secondary structure propensity analysis from experimental  $^{13}\text{C}\alpha$  and  $^{13}\text{C}\beta$  chemical shifts of NS5A-D2. Positive and negative scores indicate helical tendencies and extended regions, respectively, whereas values close to 0 indicate a fully disordered state. *d*, deviation of experimental  $^1\text{H}$ ,  $^{15}\text{N}$ -combined chemical shift values from neighbor-corrected IDP values calculated from the primary NS5A-D2 sequence. *e*, peak intensities in the  $^1\text{H}$ ,  $^{15}\text{N}$ -HSQC spectrum, shown in Fig. S1a. *f–h*, longitudinal R1 (*f*) (Hz), transverse R2 (*g*) (Hz), and heteronuclear NOE ( $^1\text{H}$ ,  $^{15}\text{N}$ ) (*h*) relaxation rates in NS5A-D2, measured at 600 MHz and 298 K. R1 and R2 were calculated by fitting peak heights in a series of spectra to a decaying exponential, using Sparky. The error bars indicate the standard error of the fit. For  $^1\text{H}$ - $^{15}\text{N}$  NOE the error bars were calculated from the root sum square of (noise/signal) in the spectra with and without saturation. *i*,  $^1\text{D}_{\text{NH}}$  dipolar couplings measured using 2D  $^{15}\text{N}$  IPAP-HSQC experiments recorded both in isotropic and anisotropic conditions. The error bars represent experimental errors, calculated from the linewidths at half-height in the  $^{15}\text{N}$  dimension and the signal to noise ratio.

3a). The W312\_1 resonance thereby corresponds to the *trans* conformation of Pro<sup>306</sup>, Pro<sup>310</sup>, Pro<sup>315</sup>, Pro<sup>319</sup>, and Pro<sup>320</sup>.

All of these Trp<sup>312</sup> resonances fall along a line and form a linear chemical shift pattern (Fig. 3). A similar spectral behavior was observed for the residue Ala<sup>313</sup> (Fig. S12), which is also part of the PW-turn motif. A linear pattern of chemical shifts was previously interpreted as a proof that this residue exists in (at least) two conformational states with distinct chemical shift environments in fast exchange on the NMR time scale (68). Even if the W312\_6 and W312\_1 resonances do not exactly match with the two pure states of this fast-exchange system, these resonances can be used as proxies for the two conforma-

tional states at the extremity of the linear chemical shift pattern. Considering the frequency difference between the W312\_1 and W312\_6 resonances ( $\Delta\omega^1\text{H} \sim 420$  Hz,  $\Delta\omega^{15}\text{N} \sim 300$  Hz), the time scale of this exchange is faster than 1–0.1 ms. Moreover, the observed line broadening or equivalent enhanced R<sup>2</sup> rates for this residue suggest that the exchange is close to this microsecond-millisecond time range.

### Allosteric regulation of the PW-turn motif by proline cis/trans equilibria

To further characterize the PW-turn in each of these distinct conformers, we analyzed the same NMR parameters as for the

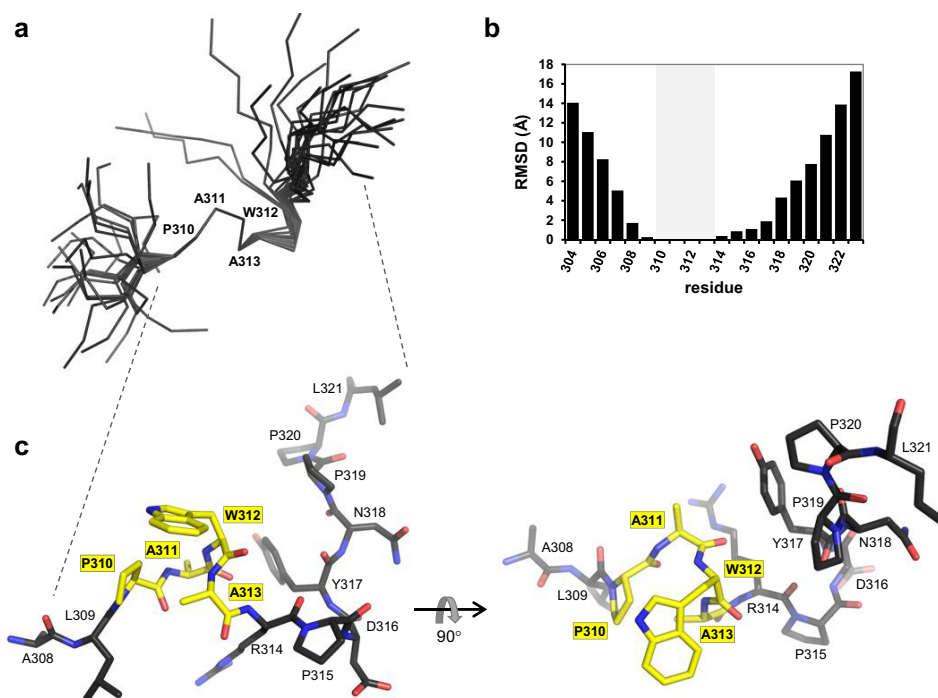


**Figure 2. Structure of the PW-turn.** *a*, superimposition of the 23 final NMR conformers of pepD2-WT (JFH1) (residues 304–323, GFPRALPAWARPDYNPPLVE), shown as C $\alpha$  traces. *b*, local r.m.s. deviation values (Å) for the backbone atoms (N, C $\alpha$ , and CO) of each residue in the final bundle of structures. The region shaded in light gray corresponds to the PW-turn motif (Pro<sup>310</sup> to Ala<sup>313</sup>). *c*, structure of the PW-turn motif (in yellow) in stick representation. Figures were prepared using PyMOL (PyMOL Molecular Graphics System, version 1.8, Schrödinger, LLC).

major all-*trans* form for the distinct conformers: deviations between experimental <sup>1</sup>H, <sup>15</sup>N-combined chemical shift or <sup>13</sup>C $\alpha$  chemical shift values and their expected neighbor-corrected random coil values, the RDC<sub>NH</sub> for each of the Trp<sup>312</sup> resonances and the difference between the proton chemical shift values of Trp<sup>312</sup> H $\beta$ 2 and H $\beta$ 3, respectively. As a result, we firmly established a linear correlation between each of these structural NMR parameters and either the <sup>1</sup>H or <sup>15</sup>N experimental chemical shift values of the Trp<sup>312</sup> resonances (Fig. 4 and Fig. S13). The left-most point (W312\_6) on the linear chemical shift pattern, corresponding to the *cis* conformer of Pro<sup>310</sup>, is close to both the Trp<sup>312</sup> resonance in the A311G mutant and to the expected position for random-coil region, whereas the experimental parameters used to derive the atomic structure of the structured PW-turn (Fig. 2) correspond to the all-*trans* right-most point (W312\_1). The position of the Trp<sup>312</sup> resonance along the linear chemical shift pattern corresponds to the population-weighted average between these two states. The folding-unfolding of the PW-turn structural motif in the disordered NS5A-D2 thus is allosterically regulated by the *cis/trans* conformation of 5 different proline residues, *i.e.* Pro<sup>306</sup>, Pro<sup>310</sup>, Pro<sup>315</sup>, Pro<sup>319</sup>, and Pro<sup>320</sup>. Adopting a *cis* conformation for any single proline residue reduces the structured population in the conformational ensemble. The impact of these *cis*-prolines on the PW-turn is not directly proportional to the distance to Trp<sup>312</sup> in the primary sequence. The *cis*-Pro<sup>319</sup> and *cis*-Pro<sup>320</sup>, which are at a distance of 7 and 8 residues, respectively, have for example a more pronounced effect on the PW-turn than the *cis*-P306 that is at a distance of 6 residues (Fig. S14). Interestingly, the three proline residues having a major effect on the structured PW-turn content, *i.e.* Pro<sup>310</sup>, Pro<sup>315</sup>, and

Pro<sup>319</sup>, respectively (Fig. 3 and Fig. S14), correspond to the ones having the most pronounced functional impact on HCV RNA replication (28).

#### CypA-inhibitor resistance mutations correspond to allosteric perturbations

The model of NS5A-D2 with a population-weighted average between a structured PW-turn motif and its disordered counterpart is further strengthened by the analysis of the NMR spectra of NS5A-D2 mutants. We examined the position of the major Trp<sup>312</sup> resonance (*i.e.* W312\_1) in the <sup>1</sup>H, <sup>15</sup>N-HSQC spectra of two NS5A-D2 mutants with CypA-inhibitor resistance mutations (D316E or D316E/Y317N (DEYN), respectively). These mutations confer to HCV a moderate resistance (~2–4-fold) to CypIs and a reduced CypA dependence (27, 41, 43, 44). Comparing them to the position of Trp<sup>312</sup> in NS5A-D2 Pro to Ala mutants (P306A, P310A, P315A, P319A, and P320A) (Fig. 5) and the A311G mutant, in which the PW-turn motif is absent (see Fig. S1b), we find that the Trp<sup>312</sup> peak in all these mutants displays a colinear chemical shift perturbation pattern (68) (Fig. 5a), which coincides with the one previously defined by the *cis* forms of individual prolines in NS5A-D2 WT (Fig. 4a). This further confirms the PW-turn as a dynamic, rapidly inter-converting ensemble wherein individual mutations directly influence the population of folded and unfolded conformers. The <sup>1</sup>H and <sup>15</sup>N chemical shift values of the Trp<sup>312</sup> resonance from the mutants correlate linearly with several structural NMR parameters (<sup>13</sup>C $\alpha$ ,  $\Delta\delta$ NH) (Fig. 5, b and c, and Fig. S15), and indicate that all but the P320A mutation reduce the population of the structured PW-turn motif in the dynamic ensemble (Fig. 5a). To verify whether the effect of the CypI-

## Conformational regulation of NS5A-D2 by CypA

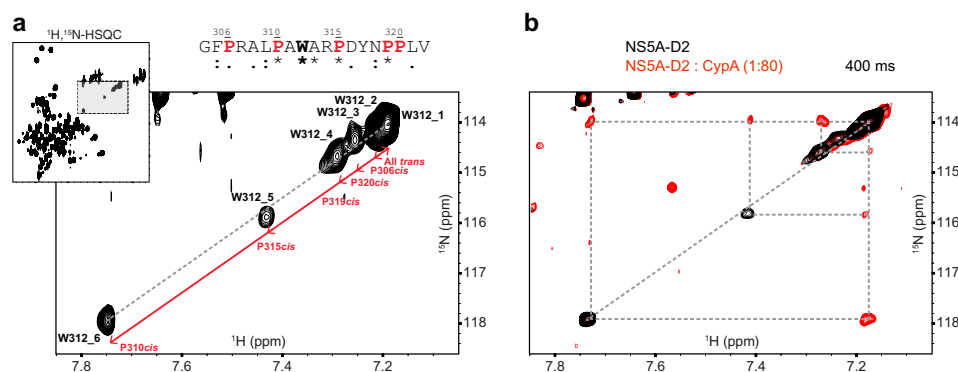


**Figure 3. A linear chemical shift pattern for Trp<sup>312</sup> and proline *cis/trans* equilibria in NS5A-D2.** *a*, zoomed-in view of the Trp<sup>312</sup>s resonances in the <sup>1</sup>H,<sup>15</sup>N-HSQC spectrum of NS5A-D2 WT (box shaded in light gray in the upper left panel). A major (W312\_1) and 5 minor (W312\_2 to W312\_6) NMR resonances were assigned to the Trp<sup>312</sup> residue, which is surrounded by 5 proline residues in the NS5A-D2 sequence (see sequence at the top). Each minor Trp<sup>312</sup> resonance arises from the *cis* conformation of one of these proline residues (indicated in red) and is in slow-exchange (red arrows), on the NMR time scale, with the main Trp<sup>312</sup> resonance when all the surrounding proline residues are in *trans*. The linear chemical shift pattern is highlighted by a dashed gray line. *b*, <sup>1</sup>H,<sup>15</sup>N-heteronuclear exchange spectra, recorded at 600 MHz, on <sup>15</sup>N-NS5A-D2 samples (400 μM) alone (mixing times of 200 ms) (in black) or in the presence of catalytic amounts of unlabeled CypA (5 μM) (mixing time of 400 ms) (in red). Exchange peaks connecting each minor Trp<sup>312</sup> resonances (W312\_2 to W312\_6) with the main one (W312\_1) are highlighted by dashed gray boxes.

resistant mutants was direct rather than indirectly mediated through an altered proline *cis/trans* ratio, we explicitly measured the *cis/trans* ratio of each proline in the pepD2-WT or its D316E counterpart (Fig. 5*d* and Fig. S16). Only minor increases of the *cis* content was measured for Pro<sup>315</sup> and Pro<sup>319</sup>, but the all-*trans* form remained the dominant fraction.

Our combined results demonstrate that the short structural PW-turn motif (<sup>310</sup>PAWA<sup>313</sup>) identified in NS5A-D2 is structurally coupled to a larger region encompassing the 304–323 residues, whereby this larger peptide can adopt a structured motif (the PW-turn) in equilibrium with a disordered conformer. Any perturbation in this region has its impact on this equilibrium (Fig. S17). The different amino acid substitutions (A311G, D316E, DEYN, P306A, P310A, P315A, P319A, and P320A) and the *cis*-proline conformation of Pro<sup>306</sup>, Pro<sup>310</sup>, Pro<sup>315</sup>, Pro<sup>319</sup>, and Pro<sup>320</sup>, all constitute a library of allosteric perturbations. We used the chemical shift projection analysis (CHESPA) method (69, 70) on the two linear chemical shift patterns described in Figs. 4*a* and 5*a*, respectively (Fig. 5*e*). To this end, W312\_6 (disordered) and W312\_1 (structured) have been considered as the extremities of the linear pattern. The projection angle ( $\cos\theta$ ) defines the direction of the perturbation and also shows if the observed residue (here Trp<sup>312</sup>) is affected by the perturbation through nearest-neighbor effects. All perturbations resulted in a  $\cos\theta$  value of  $\sim 1$ , which is expected for a linear pattern. The only exception is for the A311G mutation that has a stronger nearest-neighbor effect on the Trp<sup>312</sup> resonance. The fractional shift ( $X$ ) allows the quantification of the two states (here disordered/structured) in the presence of one of the perturbations (here, *cis*-Pro or mutations). The D316E and DEYN mutations, the *cis*-Pro<sup>315</sup> conformation, or the A311G mutation thereby correspond to ensembles wherein 82, 61, 55, or 7% of the conformers, respectively, adopt the structured PW-turn motif.

### Molecular dynamics of the PW-turn

To validate our NMR-based conclusions by an independent approach, we performed Gaussian accelerated molecular dynamics (MD) simulations ( $\sim 280$  ns, 140,000 frames) on five

20-mer peptides (pepD2-WT, -D316E, -DEYN, -A311G, and -P315*cis*). For each simulation, a dihedral principal component analysis (dPCA) (71, 72) was performed on the backbone dihedral angles ( $\phi$  and  $\psi$ ) of residues 309 to 316, and a clustering of the structures was performed using the two first vectors of the dPCA (Fig. S18*a*). The percent of the time that each cluster is present was determined. Then, using our NMR structure as a reference, we probed the presence of the PW-turn motif in every cluster of each calculation. In the MD simulations, the PW-turn motif was found in 90, 73, 66, 65, and 2% of the conformers (called the PW\_fraction) for pepD2-WT, pepD2-D316E, pepD2-DEYN, pepD2-P315*cis*, and pepD2-A311G, respectively (Fig. 6*a*). Ensemble average proton amide (<sup>1</sup>H and <sup>15</sup>N) chemical shift predictions, performed with ShiftX2 (73) on the MD structures, showed linear patterns for Trp<sup>312</sup> and Ala<sup>313</sup>, confirming the experimental observations (Fig. S18, *b* and *c*). There is a strong linear correlation between the PW\_fractions from the MD simulations and the experimental <sup>1</sup>H or <sup>15</sup>N chemical shifts of Trp<sup>312</sup> in the HSQC spectra of NS5A-D2 (Fig. 6, *b* and *c*). We also found a linear correlation ( $R^2 = 0.94$ ) between the MD PW\_fractions and the fractional shift ( $X$ ) from the CHESPA analysis (Fig. 6*d*), illustrating the validity of the model.

### The interaction with CypA is modulated by the fraction of the structured PW-turn in NS5A-D2

We have previously shown that the disruption of the structured PW-turn motif weakens 3-fold the molecular interaction between CypA and NS5A-D2 (in the context of the Con1 strain) (30). As the CypA-inhibitor resistance mutation D316E reduces the fraction of the NS5A-D2 conformers that retain this structural element (Fig. 6), the molecular interaction between NS5A-D2 D316E and CypA was assessed. Using <sup>15</sup>N-labeled CypA, NMR titration experiments were acquired with increasing amounts of unlabeled PepD2-WT, PepD2-D316E, or PepD2-A311G peptides (Fig. 7 and Fig. S19, *a–c*). The dissociation constants ( $K_D$ ) were determined from the chemical shift perturbations of CypA induced by the addition of the peptides. The affinity between CypA and PepD2-WT ( $K_D = 0.74$  mM),

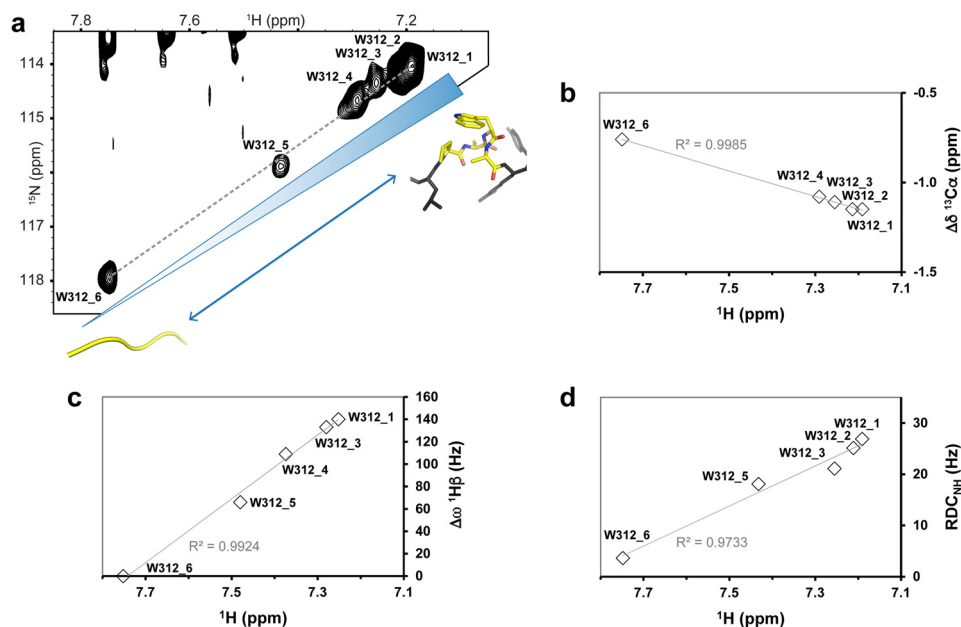


**Figure 4. Allosteric regulation of the PW-turn.** *a*, the position (*i.e.* its  $^1\text{H}$  chemical shift) of each Trp $^{312}$  resonances along the linear pattern (highlighted by a dashed gray line) in the  $^1\text{H}$ , $^{15}\text{N}$ -HSQC spectrum correlates with: the differences between experimental  $^{13}\text{C}\alpha$  chemical shift (*b*) values and their expected neighbor-corrected random coil values; the differences (in  $^1\text{H}$  ppm) between the two H $\beta$  resonances of W312 (*c*) in a  $^1\text{H}$ , $^1\text{H}$ -TOSCY experiment acquired on an unlabeled pepD2-WT (Fig. S13c); and also with its experimental NH residual dipolar coupling (*d*). There is a two-states fast-exchange between the structured PW-turn and its disorder counterpart (blue arrow in *a*). The position of the Trp $^{312}$  resonance is the population-weighted average of the pure structured and disordered states. The *cis/trans* conformation of each surrounding proline residues corresponds to an allosteric effector. The linear correlations with their corresponding correlation coefficients ( $R^2$ ) are shown in gray.

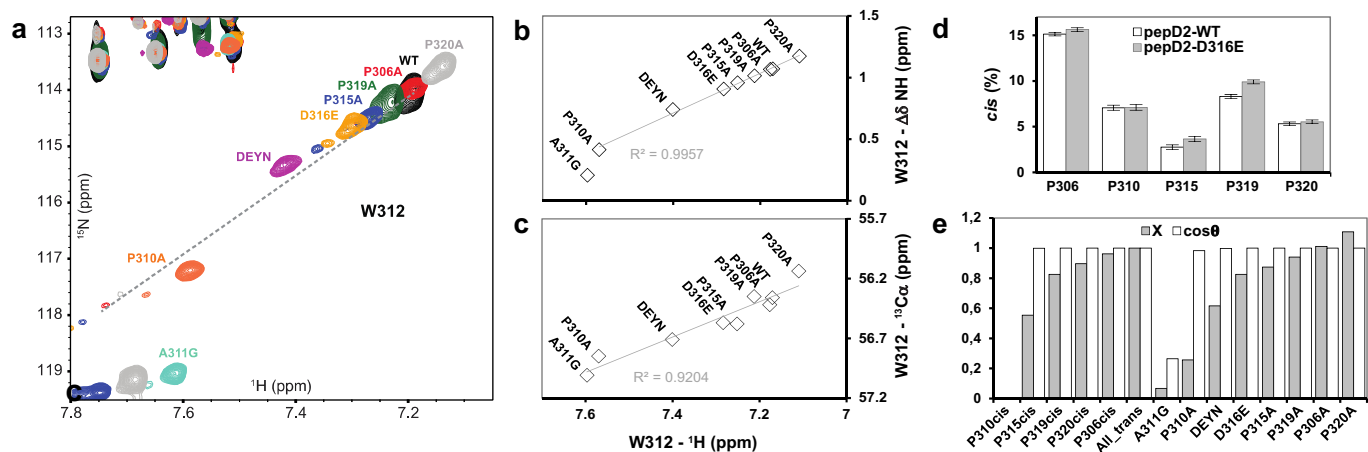


**Figure 5. Allosteric perturbations of the PW-turn.** *a*, overlay of the  $^1\text{H}$ , $^{15}\text{N}$ -HSQC spectrum of NS5A-D2 WT (in black) with that of the mutants P306A (red), P319A (green), P315A (dark blue), D316E (orange), DEYN (D316E + Y317N, violet), P310A (salmon), A311G (light blue), and P320A (light gray), respectively. The spectra are centered on the Trp $^{312}$  resonance. The linear chemical shift pattern is highlighted by a dashed gray line exactly as in Figs. 3 and 4. *b* and *c*, linear correlations between the experimental Trp $^{312}$   $^1\text{H}$  chemical shift values and (*b*) the differences between experimental and expected neighbor-corrected random coil  $^1\text{H}$ , $^{15}\text{N}$ -combined chemical shift values, or (*c*) experimental  $^{13}\text{C}\alpha$  chemical shifts, respectively. The linear correlations with their corresponding correlation coefficients ( $R^2$ ) are shown in gray. *d*, quantification of the *cis* conformation for each proline residues around Trp $^{312}$ , both in the pepD2-WT and pepD2-D316E peptides. The *cis* contents (in %) were calculated by using the peak heights of the H $\alpha$ -N resonances corresponding to the *trans* and *cis* proline conformers in  $^1\text{H}$ , $^{15}\text{N}$ -H $\alpha$ (C $\alpha$ )N experiments recorded on  $^{13}\text{N}$ , $^{13}\text{C}$ -doubly labeled peptides. Error bars were calculated based on the signal-to-noise ratio with uncertainties propagations. *e*, CHESPA analysis. Both the fractional structuration ( $X$ , gray bars) and the projection angle ( $\cos\theta$ , white bars) were calculated for the linear chemical shift patterns shown in Fig. 3 and in panel *a*, respectively. In both cases, the W312\_1 (All\_ *trans*) and W312\_6 (P310*cis*) resonances of NS5A-D2 WT were taken as the extremities of the linear patterns.

which hold the structured PW-turn, is  $\sim 2$  times higher than the one with the fully disordered PepD2-A311G peptide ( $K_D = 1.37$  mM). These affinities are similar to the ones that we have previously measured between CypA and similar peptides derived from the HCV Con1 strain (0.53 and 1.38 mM, respectively) (30). With respect to the interaction between CypA and the peptide pepD2-D316E, an intermediate  $K_D$  value of 1.18 mM was measured. The affinities between CypA and the NS5A-D2-derived peptides, even being in the same order of magnitude, are correlated with the

fraction of the conformers that own the structured PW-turn motif in the NS5A-D2 ensemble, as determined by NMR spectroscopy and MD simulations (Fig. S19, *d* and *e*).

#### The fraction of structured PW-turn motif in NS5A-D2 ensemble tunes the HCV replication level

The PW-turn motif in NS5A-D2 is essential for HCV RNA replication (10, 30), but has the dynamic equilibrium between the structured and disordered states that we identified in this

## Conformational regulation of NS5A-D2 by CypA

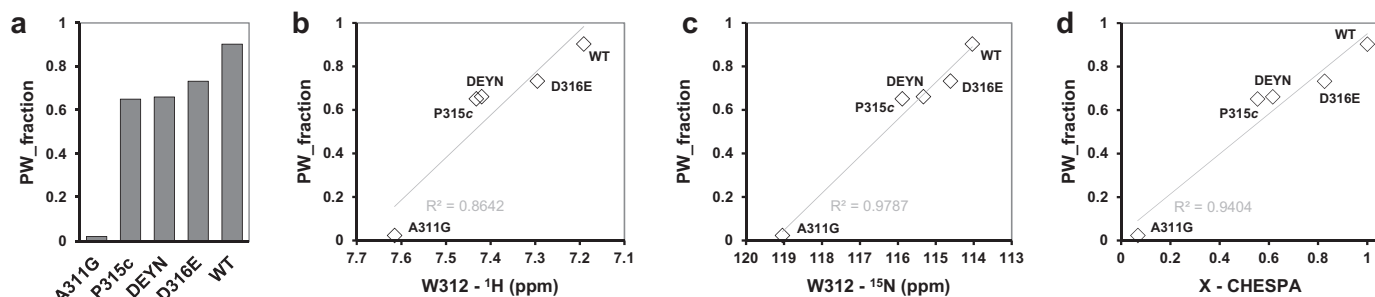


**Figure 6. Molecular dynamics of the PW-turn.** *a*, MD simulations were performed on peptides pepD2-WT (WT), pepD2-D316E (D316E), pepD2-DEYN (DEYN), pepD2-P315cis (P325c), and pepD2-A311G (A311G). The presence of the PW-turn motif (PW\_fraction) in each simulation was quantified as described under “Experimental procedures,” using our NMR structural model as a reference. *b* and *c*, plots of the PW\_fraction of each peptide, from MD simulations, versus the experimental Trp<sup>312</sup> <sup>1</sup>H (*b*) or <sup>15</sup>N (*c*) chemical shift. *d*, plot of the PW\_fraction from MD simulations versus the fractional shift (X) from the NMR CHESPA analysis. The linear correlations with their respective correlation coefficients (R<sup>2</sup>) are shown in gray.

study have any functional relevance? To address this question, we measured the replication of subgenomic HCV replicons (JFH1 strain) encoding a firefly luciferase gene. These replicon RNAs were transfected into Huh-7 cells and replication was determined by quantifying luciferase in lysates of cells that were harvested at different time points after transfection. We have earlier shown that luciferase activity is a direct measure of viral RNA replication with the 4-h value serving as baseline because it reflects transfection efficiency. To study the importance of the equilibrium shift of the PW-turn motif, we compared replication capacity of the wildtype (WT) replicon or replicon variants containing distinct mutations in NS5A-D2 (A311G, P310A, DEYN, and A311I) (Fig. 8*a*). The A311G substitution in NS5A reduced RNA replication to background levels as determined with the replication-dead replicon encoding an enzymatically inactive NS5B polymerase (mutant ΔGDD). By contrast, the replication efficiency of the A311I mutant was similar to that of the NS5A-WT consistent with the notion that the structural PW-turn motif in the disordered NS5A-D2 domain is essential for viral RNA replication. Indeed, in the HCV Con1 strain, position 311 corresponds to an isoleucine residue (30). Mutations P310A and DEYN in NS5A affected RNA replication, showing phenotypes intermediate between those of the WT and A311G mutant. Of note, we found a striking correlation between RNA replication efficiencies measured *in cellulo* and the NMR data acquired on purified NS5A-D2 *in vitro* (Fig. 8, *b* and *c*, and Fig. S20). Indeed, RNA replication levels of NS5A WT and its NS5A mutants correlate with the position (<sup>1</sup>H and <sup>15</sup>N) of the Trp<sup>312</sup> resonance in their corresponding <sup>1</sup>H,<sup>15</sup>N-HSQC spectra. This strong correlation suggests that the structured PW-turn motif in the NS5A-D2 ensemble is required for robust HCV RNA replication, provided the CypA PPIase activity allows to reach, on a subsecond time scale, subensembles in which the structured PW-turn population is reduced. It means that the conformational equilibrium of the PW-turn motif in NS5A-D2 has to be finely regulated to be fully functional. Hence, our data also provide an explanation for the striking antiviral potency of CypIs.

### Discussion

RNA replication, a central step in the HCV life cycle, requires the formation of a replication complex that includes the viral NS5B and NS5A proteins associated to membrane structures

(DMVs) (7, 74). NS5B with its RNA-dependent RNA-polymerase activity (8) is the catalytic core of this functional complex. In contrast, the absence of measurable enzymatic activity and the presence, alongside its first well-structured domain (11, 20, 21), of two intrinsically disordered domains (NS5A-D2 and -D3) (17–19), make the role of NS5A in the HCV replicase much less obvious. Human CypA, as an essential cellular protein required for the viral replication process (75), has been functionally linked to NS5A-D2 by the accumulation of CypI-resistance mutations in this disordered domain (41, 76), and by the identification of a physical interaction between these two proteins (25, 37). However, the role(s) of these two proteins in the replication of HCV remains elusive, which is in part because the PPIase activity and the binding properties of CypA cannot be uncoupled.

The precise role of human cyclophilins in a viral life cycle has been best studied in the context of HIV capsid (de)stabilization (77). CypA is incorporated into newly produced HIV virions through its interaction with a proline-rich loop (CypA-loop) in the viral capsid protein (CA) (78–80). Although the Pro<sup>90</sup> residue in CA is required for both the interaction with CypA and viral replication, the importance of other surrounding proline residues (Pro<sup>85</sup>, Pro<sup>93</sup>, and Pro<sup>99</sup>) in viral replication was also pointed out (79). CypA displays *in vitro* catalytic PPIase activity toward the Gly<sup>89</sup>–Pro<sup>90</sup> peptidyl bond in the CypA-loop of the CA protein in the intact HIV-1 virion (81), but the functional role of this activity remains uncertain. CA mutations such as A92E and G94D, obtained during HIV-1 passage in HeLa cells under CypA inhibition (82), allow these HIV-1 mutants to escape CypA dependence, without altering the interaction with CypA (83). However, the infectivity of these mutants drops by 90% in HeLa cells, which could be fully recovered upon CypA inhibition (83). Recently, it has been reported that the CypA-loop of the A92E and G94D CA mutants in the assembled capsid structures adopts comparable dynamics as the loop in the WT CA when bound to CypA (84). Hence, both selected resistance mutations and CypA binding seemingly lead to the same dynamic effect on this CA loop, but cannot be combined without the risk of overshooting the dynamical requirements for optimal infectivity. Along these lines, the rhesus monkey Trim5α induces global attenuation of the capsid dynamics even beyond the CA loop and may ultimately promote its disassem-

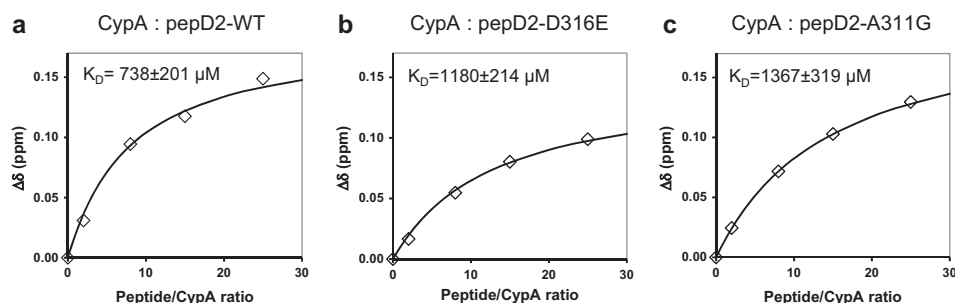


**Figure 7. Interaction of CypA with NS5A-D2-derived peptides: pepD2-WT (a), pepD2-D316E (b), and pepD2-A311G (c).**  $^1\text{H}$ ,  $^{15}\text{N}$ -HSQC spectra of  $^{15}\text{N}$ -CypA (0.1 mM) were acquired in the presence of increasing amounts of unlabeled NS5A-D2 derived peptides (0, 0.2, 0.8, 1.5, and 2.5 mM). The CypA  $^1\text{H}$ ,  $^{15}\text{N}$  combined chemical shift perturbations ( $\Delta\delta$ , ppm) are plotted as a function of the peptide/CypA ratios. The  $K_D$  values correspond to the mean ( $\pm$  S.D.) calculated over five CypA resonances (Ile<sup>56</sup>, Leu<sup>98</sup>, Met<sup>100</sup>, Ser<sup>110</sup>, and Gly<sup>124</sup>) (Fig. S19).

bly (85). From these data on HIV-1 CA-CypA interaction, one can conclude that fine tuning of dynamical aspects of viral proteins (here CA) is an additional mean used by viruses to optimize infectivity.

Our present work on HCV NS5A-D2 and its relationship with CypA points toward the same direction. We detect the PW-turn structural motif in the mainly disordered NS5A-D2 domain from the HCV JFH-1 strain (Figs. 1 and 2), thereby confirming our previous results in the Con1 strain (30). Moreover, we show that the structural motif extends beyond the  $^{310}\text{PAWA}^{313}$  sequence to include at least 4 more proline residues (Pro<sup>306</sup>, Pro<sup>315</sup>, Pro<sup>319</sup>, and Pro<sup>320</sup>) (Fig. 3 and Fig. S17). However, this motif is not static. Using NMR chemical shifts as atomic resolution sensors, we demonstrate that the PW-turn motif exists as an equilibrium between two states, a structured state and a disordered state, which interconvert in fast exchange on the NMR time scale (Fig. 4). This equilibrium, probed via the Trp<sup>312</sup> resonance, is modulated by the *cis/trans* equilibria of the 5 surrounding prolines (Pro<sup>306</sup>, Pro<sup>310</sup>, Pro<sup>315</sup>, Pro<sup>319</sup>, and Pro<sup>320</sup>). This translates into one major and 5 minor resonances for the Trp<sup>312</sup> amide function that make a linear chemical shift pattern in the  $^1\text{H}$ ,  $^{15}\text{N}$ -HSQC of NS5A-D2 WT (Figs. 4 and 5). The linear pattern is bordered on the structured side by the all-*trans* form used to derive the structure of the PW-turn (Fig. 3), and by the *cis*-Pro<sup>310</sup> form on the almost completely disordered side (Figs. 3 and 4). As these different equilibria are separated by the conformation (*trans* or *cis*) of distinct prolyl bonds, they are separated by the slow time scale of the spontaneous *cis/trans* isomerization of each of these bonds. CypA can lower this barrier through its PPIase activity, and thereby connect these different ensembles at a subsecond time scale (Fig. 3b) (25, 30). As such, the PPIase activity of CypA do not alter the folded and unfolded states of the PW-turn but rather allows fast reach to the NS5A-D2 subensembles in which the structured PW-turn population is reduced (Fig. S21). The CypI resistance mutations in NS5A-D2, D316E, or DEYN lead to a similar effect as they reduce the population of the structured PW-turn motif in the dynamic ensemble (Fig. 5 and Fig. S21). The folded conformer population, with all prolines in *trans*, drops from nearly  $\sim 100\%$  in NS5A-D2 WT to 82% in the D316E mutant (*i.e.* the same population as in the *cis*-Pro<sup>319</sup> subensemble in the WT), and to 62% in the DEYN mutant (comparable with that of the *cis*-Pro<sup>315</sup> subensemble in the WT) (Figs. 3 and 5). Both mutations confer some CypA inde-

pendence, but lower the replication level when measured in cell lines where CypA is present (27, 41, 43, 44). Moreover, in a similar way to what was observed for the mutations in the CypA-loop of HIV-1 CA, the replication capacity of the DEYN HCV mutant has been shown to be higher when CypA was silenced (28). As the Trp<sup>312</sup> chemical shift ( $^1\text{H}$  and  $^{15}\text{N}$ ) of the mutants correlates linearly with the RNA replication efficiency ( $\log_{10}$  scale) in a cell-based assay (Fig. 8), we conclude that CypA is fine tuning the dynamics of the PW-turn motif in NS5A-D2.

The relationships involving CypA/CA from HIV-1 or CypA/NS5A-D2 from HCV are strikingly similar. A short sequence involving a conserved proline residue constitutes the CypA-binding site (Gly<sup>89</sup>-Pro<sup>90</sup> or  $^{310}\text{PAWA}^{312}$ , respectively); the residues C-terminal to this binding site trigger peculiar conformational properties and are involved in the replication efficiency of the viruses; CypI-resistance mutations conferring (partial) relief of the CypA-dependence are localized next to the CypA-binding site; and finally, CypA exerts a fine modulation of the dynamics of the viral proteins (the CypA-loop of CA or the PW-turn motif in NS5A-D2). HIV-1 and HCV seem to have evolved to use the host CypA as a fine-tuning rheostat, which allows them to keep their functional systems in a rather sharp optimal window. Finally, in the presence of the CypI-resistance mutations, CypA is detrimental as it over-attenuates the dynamics of the CypA-loop in HIV-1 CA or it over-reduces the fraction of the PW-turn in HCV NS5A.

Whereas we show that the fraction of the structured PW-turn motif in the NS5A-D2 conformational ensemble, which is allosterically regulated by both the *cis/trans* isomerization of 5 prolines residues (Pro<sup>306</sup>, Pro<sup>310</sup>, Pro<sup>315</sup>, Pro<sup>319</sup>, and Pro<sup>320</sup>) and by CypI-resistance mutations, correlates with the HCV RNA replication efficiency (Fig. 8), the question of how a structured PW-turn motif in NS5A-D2 contributes to viral replication remains open. NS5A was shown to play a role in the formation of DMVs and functional replication complexes contained therein, through remodeling the ER membrane, and CypI could interfere with this role for NS5A. Alternatively, NS5A-D2 directly interacts with the dynamic molecular machine that is the NS5B RNA polymerase (86), and thereby might allosterically regulate its RNA binding (15) and/or enzymatic activity (87). Different conformational ensembles of the disordered NS5A-D2, with varying fractions of (un)folded PW-turn motif, might be required for

## Conformational regulation of NS5A-D2 by CypA

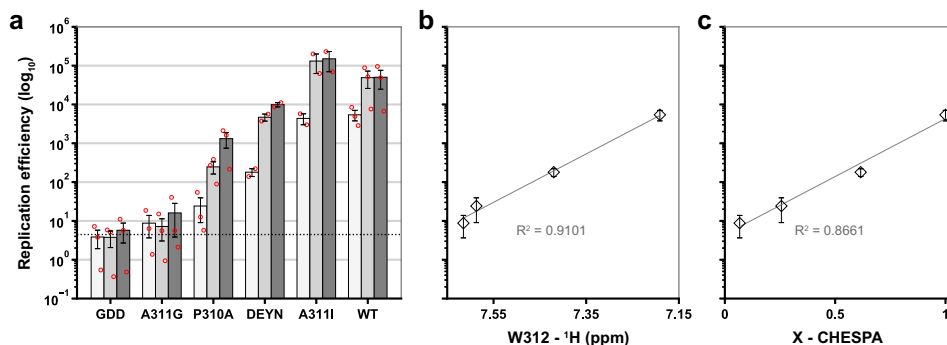


**Figure 8. Functional relevance of the PW-turn.** *a*, subgenomic JFH1 replicons (Luc-NS3–5B) containing or not (WT) single mutations (A311G, P310A, DEYN, or A311I) in NS5A or a defective polymerase inhibiting replication ( $\Delta$ GDD) were electroporated into Huh-7 cells. The cells were lysed 4, 24, 48, and 72 h after transfection and luciferase activity (representing RNA replication) was measured. The data were normalized to their respective 4-h value reflecting transfection efficiency. Mean  $\pm$  S.E. of 3 independent experiments ( $n = 3$ ) are shown (2 independent experiments for the A311I and DEYN mutants). The horizontal dashed line corresponds to the background level as determined with the  $\Delta$ GDD replicon. *b* and *c*, plots of the RNA replication efficiencies (*i.e.* luciferase activity values, of the different subgenomic replicons in *a*) versus the experimental Trp<sup>312</sup> <sup>1</sup>H chemical shift (*b*) or the fractional shift (X) from the NMR CHESPA analysis (*c*). The exponential correlations with their respective coefficients ( $R^2$ ) are shown in gray.

these multiple functional roles. Our present data add further complexity to this picture, whereby allosteric regulation of the NS5A-D2 domain through its proline conformations might be modulated by the enzymatic function of the host factor CypA. Simultaneously, although, it shows that targeting the dynamical aspects of viral protein(s) can open new avenues in the discovery of antivirals.

### Experimental procedures

#### Expression and purification of NS5A-D2 and CypA

The synthetic sequence coding for domain 2 of the HCV NS5A protein from JFH1 strain (GenBank<sup>TM</sup> accession number AB047639, genotype 2a) was introduced in the bacterial expression vector pT7.7 with a His<sub>6</sub> tag. The resulting recombinant domain 2 of HCV NS5A (NS5A-D2; residues 248–341) has extra M- and -LQH HHHHHH extensions at the N and C termini, respectively. The NS5A-D2 mutants (A311G, P306A, P310A, P315A, P319A, P320A, C298S/C338S/M254C, C298S, C338S, D316E, D316E/Y317N) were generated by site-directed mutagenesis on the pT7-7-NS5A-D2 WT plasmid using the forward and reverse primers listed in Table S1. The expression, in *Escherichia coli* BL21(DE3), and purification of <sup>15</sup>N (or <sup>15</sup>N,<sup>13</sup>C)-labeled NS5A-D2 was performed as previously described (25, 30). The production and purification of both unlabeled and <sup>15</sup>N-labeled CypA were performed as previously described by Hanouille and co-workers (25).

#### NS5A-D2–derived peptides

<sup>15</sup>N,<sup>13</sup>C-labeled peptides (PepD2-WT (GFPRALPAWARPDYNPPLVE), PepD2-A311G (GFPRALPGWARPDYNPPLVE), and PepD2-D316E (GFPRALPAWARPEYNPPLVE)) corresponding to residues 304–323 of NS5A-D2 JFH1 were produced as fusion proteins in *E. coli*, cleaved, and then purified as described previously (30). The resulting <sup>15</sup>N,<sup>13</sup>C-labeled PepD2-WT, PepD2-A311G, and PepD2-D316E peptides thus contain an extra N-terminal proline residue resulting from the DP chemical-cleavage site. The unlabeled peptides (PepD2-WT, PepD2-A311G, and PepD2-D316E) were purchased from Genecust (Luxembourg).

#### Conservation of NS5A-D2 sequence among HCV genotypes

The NS5A-D2 sequence from the HCV JFH1 strain (AB047639, genotype 2a) is numbered as in the full-length NS5A protein. The amino acid repertoire was deduced from the ClustalW multiple alignments of 28 representative NS5A sequences from all confirmed HCV genotypes and subtypes (see the European HCV Database (88)) using the Network Protein Sequence Analysis webserver tools (89). Amino acids observed at a given position in less than two distinct sequences are not included. The degree of amino acid conservation at each position can be inferred from the extent of variability (with the observed amino acid listed in decreasing order of frequency from top to bottom) together with the similarity index according to ClustalW convention (asterisk, invariant; colon, highly similar; dot, similar).

#### NMR spectroscopy

All NMR experiments were performed at 298 K using Bruker Avance 600 MHz or 900 MHz NMR spectrometers, both equipped with a cryogenic triple resonance probe (Bruker, Karlsruhe, Germany). The proton chemical shifts were referenced using the methyl signal of TMSP (sodium 3-trimethylsilyl-[2,2,3,3-*d*<sub>4</sub>]propionate) at 0 ppm. Spectra were processed and analyzed with the Bruker TopSpin software package 3.2. Data analysis, peak picking, and calculation of peak volumes were done with Sparky software (90).

Assignments of NS5A-D2 JFH1 (WT) backbone resonances were taken from Ref. 25 (BMRB accession code 16165). Two NMR datasets were acquired on each peptide (PepD2-WT, PepD2-A311G, and PepD2-D316E). The first set, which contains <sup>1</sup>H-<sup>1</sup>H TOCSY, <sup>1</sup>H-<sup>1</sup>H NOESY, and <sup>1</sup>H-<sup>15</sup>N HSQC spectra at 600 MHz were acquired on the unlabeled peptides at natural abundance. The second dataset was acquired on uniformly <sup>15</sup>N,<sup>13</sup>C-labeled peptide and comprises <sup>1</sup>H-<sup>15</sup>N HSQC and three-dimensional HNCACB, HN(CO)CACB, HNCO, and HNHA spectra. Assignment of PepD2-WT, PepD2-A311G, and PepD2-D316E were performed both manually and using an in-house software based on the product plane approach (91).

The  $^1\text{H}$ ,  $^{15}\text{N}$ -combined chemical shift perturbations were calculated using Equation 1, whereby  $\Delta\delta$  ( $^1\text{HN}$ ) and  $\Delta\delta$  ( $^{15}\text{N}$ ) are the chemical shift perturbations in the  $^1\text{H}$  and  $^{15}\text{N}$  dimensions, respectively. The normalization factor of 0.08 for the nitrogen frequency shift derives here from the ratio of the maximum proton frequency shift over the maximum nitrogen frequency shift.

$$\Delta\delta = |\Delta\delta(^1\text{HN})| + 0.08 \times |\Delta\delta(^{15}\text{N})| \quad (\text{Eq. 1})$$

### Residual dipolar couplings measurements

The RDCs were collected on a 100  $\mu\text{M}$  sample of  $^{15}\text{N}$  NS5A-D2 aligned in a liquid crystalline medium consisting of 6.6% (w/v) polyoxyethylene 5-lauryl ether ( $\text{C}_{12}\text{E}_5$ ) and 3% (w/v) 1-hexanol (Sigma), yielding a  $\text{D}_2\text{O}$  splitting of 35 Hz.  $^1\text{D}_{\text{NH}}$  dipolar couplings were measured on a Bruker Avance III 900 MHz spectrometer equipped with a cryogenic triple resonance probe, using 2D  $^{15}\text{N}$  IPAP-HSQC experiments (92), which allow the spin coupling measurements in the  $^{15}\text{N}$  dimension. The difference between the couplings acquired either in isotropic or anisotropic media were calculated to get the RDCs.

### Spin relaxation experiments

$^{15}\text{N}$   $\text{R}^1$ ,  $^{15}\text{N}$   $\text{R}^2$ , and  $^1\text{H}$ - $^{15}\text{N}$  NOE measurements were acquired at 600 MHz  $^1\text{H}$  frequency.  $^{15}\text{N}$   $\text{R}^1$  values were measured from spectra recorded with 10 different delays ( $T = 10, 100, 200, 400, 600, 800, 1000, 1200, 1500,$  and  $2000$  ms).  $^{15}\text{N}$   $\text{R}^2$  values were determined from spectra recorded with 11 different delays ( $T = 15.77, 31.54, 47.31, 63.08, 78.85, 94.62, 126.16, 157.7, 189.24, 220.78,$  and  $252.32$  ms). The spin echo consisted of a train of  $^{15}\text{N}$  hard  $\pi$  pulses (82  $\mu\text{s}$ ) separated by a 900- $\mu\text{s}$  inter-pulse delay. In the  $^{15}\text{N}$   $\text{R}^1$  and  $^{15}\text{N}$   $\text{R}^2$  experiments, a relaxation delay of 1 s was applied.  $^1\text{H}$ - $^{15}\text{N}$  NOE values were determined from spectra recorded either in the presence or absence of a proton pre-saturation period of 3 s, and a relaxation delay of 5 s.

### NMR structure calculation

The NMR structure calculation was performed as previously described in Ref. 30. From the different NMR datasets acquired both on unlabeled and  $^{15}\text{N}$ ,  $^{13}\text{C}$ -labeled peptide PepD2-WT (residues 304–323, JFH1), distance-based (NOEs) and backbone dihedral angle-based experimental restraints were derived. NOE intensities used as input for structure calculations were obtained from the NOESY spectrum recorded with a 400-ms mixing time. According to their intensity NOEs were classified in three categories, which were then converted into distance restraints (1.8–2.8 Å, 1.8–3.9 Å, and 1.8–5.0 Å). Protons without stereospecific assignments were treated as pseudo-atoms. From the  $^1\text{H}$ ,  $^{15}\text{N}$ , and  $^{13}\text{C}$  chemical shifts, dihedral angle constraints, calculated with Talos (93), were introduced. Peptide structures were generated from the experimental NOE distances and dihedral angles, using CNS (94) with the standard torsion angle molecular dynamics protocol, the standard force field and default parameter set. From the initial set of 100 structures that were calculated, with the dynamical annealing protocol to widely sample the conformational space, only structures with no distance restraint violations were retained. The 23

final selected structures, with the lowest energies, were compared by pairwise root mean square deviation over the backbone atom coordinates (N, C $\alpha$ , and C'). Ramachandran analysis performed on the final structures showed that 89, 11, and 0% of the residues were in favored, allowed, and outliers regions, respectively. The PyMOL software (PyMOL Molecular Graphics System, version 1.8; Schrödinger) was used for molecular graphics (95).

### NMR PPIase assay

PPIase activity of CypA on NS5A-D2 WT was assessed using  $^1\text{H}$ ,  $^{15}\text{N}$  z-exchange spectra (66), where the exchange was monitored on the basis of novel cross-peaks connecting a *trans* and *cis* peak.  $^1\text{H}$ ,  $^{15}\text{N}$  z-exchange spectra, with a 200- or 400-ms mixing time, were recorded on a 600 MHz spectrometer equipped with a cryogenic triple resonance probe. Exchange spectra were acquired on a 400  $\mu\text{M}$   $^{15}\text{N}$ -NS5A-D2 sample in the presence or the absence of 5  $\mu\text{M}$  CypA in 30 mM  $\text{NaH}_2\text{PO}_4$ /  $\text{Na}_2\text{HPO}_4$ , pH 6.4, 30 mM NaCl, 1 mM DTT.

### Chemical shift projection analysis (CHESPA)

The NMR chemical shift projection analysis was performed as described in Refs. 69 and 70, from the  $^1\text{H}$ ,  $^{15}\text{N}$ -HSQC of NS5A-D2. We calculated  $\cos\theta$ , which represents the angle between vectors A (defined by the W312\_6 and W312\_1 peaks) and B (defined by the W312\_6 peak and the Trp<sup>312</sup> resonance from a mutant or corresponding to a minor form). Next, we calculated the fractional shift X, which corresponds to the projection of the vector B on the vector A. For the calculations, a scaling factor of 0.1 was applied to the  $^{15}\text{N}$  chemical shift.

### Molecular dynamics

Gaussian-accelerated molecular dynamics (GaMD) simulations (~280 ns) were performed with AMBER17 (96, 97) on five different peptides corresponding to the 304–323 residues in NS5A-D2 (pepD2-WT (WT), pepD2-D316E (D316E), pepD2-DEYN (DEYN), pepD2-P315*cis* (P325c), and pepD2-A311G (A311G)), and each trajectory was collected with ~140,000 frames. The detailed molecular dynamics protocol is described under the supporting information.

Briefly, the peptides were built using Tleap in AmberTools16 and all simulations were performed using pmemd.cuda of AMBER17 on graphics processing units P100 (98). Amber ff99SB\*-ILDN force field (99, 100) was used in all simulations. The peptides were then solvated in a cubic water box of  $75.5 \times 75.5 \times 75.5 \text{ \AA}^3$  pre-equilibrated TIP3P water molecules. The simulations were performed with 40 mM NaCl at 298 K, as in the experimental NMR studies. GaMD (101) simulations (~280 ns) were used to explore the conformational space of the peptides and the coordinates were saved every 2 ps. CPPTRAJ (1) was used to analyze r.m.s. deviations, secondary structure, dihedral torsions, and hydrogen bonds from the GaMD simulation trajectories. The sampled conformations of the peptides were analyzed using the dPCA method (71, 72) considering the backbone atoms of residues 309 to 316. The lowest energy conformations were identified by projecting the trajectories of the first two principal components onto a three-dimensional free energy ( $\Delta G$ ) (see Equation 2 below), in which  $R$  is the universal

## Conformational regulation of NS5A-D2 by CypA

gas constant,  $T$  is the temperature,  $x$ ,  $y$ , and  $z$ , are the calculated structural properties from the trajectory.

$$\Delta G = -RT \ln \left( \frac{P_{x,y,z}}{P_{\max}} \right) \quad (\text{Eq. 2})$$

Then, a clustering of the structures was performed using the two first vectors (PC1 and PC2) of the dPCA. For each MD simulation, the PyReweight toolkit was used to reweight the GaMD simulation to compute the free energy landscape from PCA components PC1 and PC2. The percent of the time that a particular cluster is present was determined. Next, using our NMR PepD2-WT structure as a reference, the presence of the structured PW-turn motif was probed in every cluster of each simulation. For clusters of each simulations, the centroid structures were fitted on the NMR reference structure using all atoms of residues 310–313. Then, backbone dihedral angles ( $\phi$  and  $\psi$ ) of residues 310 to 313 and  $\chi_1$  and  $\chi_2$  angles from Trp<sup>312</sup> were measured using cpptraj in AMBER package. The presence of the structured PW-turn motif was assessed from the sum of squares of the differences between angles from the reference and centroid structures. Chemical shift predictions ( $^1\text{H}$  and  $^{15}\text{N}$ ) were performed with SHIFTX2 (73) from the MD simulations data. For each peptide, SHIFTX2 was used in the “ensemble mode” on all structures of each cluster. Then, from these predictions for a given peptide, a population-weighted average chemical shift value ( $^1\text{H}$  or  $^{15}\text{N}$ ) was calculated. The error bars represent the population-weighted standard deviations.

### RNA replication assay

The protocol used for generation and electroporation of HCV RNAs has been described elsewhere (38). For transient replication assays, 400  $\mu\text{l}$  of single cell suspensions of Huh-7 cells ( $10^7$  cells/ml) were mixed with 5  $\mu\text{g}$  *in vitro* transcribed subgenomic replicon RNA and transfected by electroporation. After transfection, cells were resuspended in 41 ml of complete Dulbecco's modified Eagle's medium, and 1.5 ml of the cell suspension was seeded in duplicate in each well of a 12-well plate. To measure luciferase activity, cells were washed with PBS 4, 24, 48, and 72 h after electroporation and lysed by addition of 350  $\mu\text{l}$  of lysis buffer (0.1% Triton X-100, 25 mM glycylglycine, pH 7.8, 15 mM  $\text{MgSO}_4$ , 4 mM EGTA, and 1 mM DTT). Lysates were immediately frozen at  $-70^\circ\text{C}$ , and after thawing, 100  $\mu\text{l}$  of the lysate was mixed with 360  $\mu\text{l}$  of assay buffer (25 mM glycylglycine, 15 mM  $\text{MgSO}_4$ , 4 mM EGTA, 1 mM DTT, 2 mM ATP, and 15 mM  $\text{K}_2\text{PO}_4$ , pH 7.8). Luciferase activity was measured for 20 s in a luminometer (Lumat LB9507; Berthold, Freiburg, Germany) after addition of 200  $\mu\text{l}$  of luciferin solution (200 mM luciferin, 25 mM glycylglycine, pH 8.0). Replication efficiency was calculated by normalizing values of the different time points to the respective value obtained at 4 h, which reflects transfection efficiency.

### Interaction between CypA- and NS5A-D2-derived peptides

To study the interaction between CypA and PepD2-WT, PepD2-A311G, or PepD2-D316E,  $^1\text{H}$ ,  $^{15}\text{N}$ -HSQC experiments were acquired on 400  $\mu\text{M}$   $^{15}\text{N}$ -CypA with increasing amounts of unlabeled peptides (the molar ratios CypA:PepD2 were 1:2; 1:8;

1:15, and 1:25). The combined chemical shift perturbations following peptide additions were calculated using Equation 3, whereby  $\Delta\delta$  ( $^1\text{H}$ N) and  $\Delta\delta$  ( $^{15}\text{N}$ ) are the chemical shift perturbations in the  $^1\text{H}$  and  $^{15}\text{N}$  dimensions, respectively.

$$\Delta\delta = |\Delta\delta(^1\text{H}\text{N})| + 0.2 \times |\Delta\delta(^{15}\text{N})| \quad (\text{Eq. 3})$$

For determination of dissociation constant ( $K_D$ ), the combined chemical shift perturbations ( $\delta\Delta$ , ppm) were plotted as a function of the molar ratio [PepD2]/[ $^{15}\text{N}$ -CypA], and the resulting curve was fitted to Equation 4, which describes a 1:1 biomolecular interaction, and where  $\Delta\delta$  is the measured chemical shift perturbation,  $\Delta\delta_{\max}$  is the maximum value for this parameter,  $X$  corresponds to the ratio [PepD2]/[ $^{15}\text{N}$ -CypA], and [CypA] is the  $^{15}\text{N}$ -CypA concentration.

$$\Delta\delta = \frac{\Delta\delta_{\max}}{2} \times \left( 1 + X + \frac{K_D}{[\text{CypA}]} - \sqrt{\left( 1 + X + \frac{K_D}{[\text{CypA}]} \right)^2 - 4 \times X} \right) \quad (\text{Eq. 4})$$

### Accession numbers

NMR assignment of the peptide PepD2-WT (residues 304–323 of the domain 2 of NS5A, JFH1 strain) have been deposited in the Biological Magnetic Resonance Data Bank under accession code 30037. The NMR structure of the pepD2-WT (strain JFH-1) has been deposited in the Protein Data Bank (PDB) with code 6HT4.

**Author contributions**—M. D., V. M., and I. H. resources; M. D., V. M., N. S. G., F.-X. C., H. L., I. H., and G. L. formal analysis; M. D., V. M., N. S. G., and X. H. validation; M. D., V. M., N. S. G., F.-X. C., H. L., I. H., G. L., and X. H. investigation; M. D., N. S. G., H. L., and I. H. methodology; F.-X. C. and H. L. data curation; R. B., G. L., and X. H. conceptualization; R. B. and X. H. supervision; R. B., G. L., and X. H. writing-original draft; X. H. funding acquisition; X. H. project administration.

**Acknowledgments**—The NMR facility was supported by the European Community, the CNRS (IR RMN THC, FR-3050), University of Lille, the Région Hauts-de-France (France), and the Pasteur Institute of Lille (IPL).

### References

1. Roe, D. R., and Cheatham, T. E., 3rd (2018) Parallelization of CPPTRAJ enables large scale analysis of molecular dynamics trajectory data. *J. Comput. Chem.* **39**, 2110–2117 [CrossRef Medline](#)
2. Stanaway, J. D., Flaxman, A. D., Naghavi, M., Fitzmaurice, C., Vos, T., Abubakar, I., Abu-Raddad, L. J., Assadi, R., Bhala, N., Cowie, B., Forouzanfar, M. H., Groeger, J., Hanafiah, K. M., Jacobsen, K. H., James, S. L., et al. (2016) The global burden of viral hepatitis from 1990 to 2013: findings from the Global Burden of Disease Study 2013. *The Lancet* **388**, 1081–1088 [CrossRef](#)
3. Moradpour, D., Penin, F., and Rice, C. M. (2007) Replication of hepatitis C virus. *Nat. Rev. Microbiol.* **5**, 453–463 [CrossRef Medline](#)
4. Moradpour, D., and Penin, F. (2013) Hepatitis C virus proteins: from structure to function. *Curr. Top. Microbiol. Immunol.* **369**, 113–142 [Medline](#)
5. Lohmann, V., Körner, F., Koch, J., Herian, U., Theilmann, L., and Bartenschlager, R. (1999) Replication of subgenomic hepatitis C virus RNAs in a hepatoma cell line. *Science* **285**, 110–113 [CrossRef Medline](#)

6. Romero-Brey, I., Merz, A., Chiramel, A., Lee, J.-Y., Chlanda, P., Haselman, U., Santarella-Mellwig, R., Habermann, A., Hoppe, S., Kallis, S., Walther, P., Antony, C., Krijnse-Locker, J., and Bartenschlager, R. (2012) Three-dimensional architecture and biogenesis of membrane structures associated with Hepatitis C Virus replication. *PLoS Pathog.* **8**, e1003056 [CrossRef Medline](#)
7. Paul, D., Hoppe, S., Saher, G., Krijnse-Locker, J., and Bartenschlager, R. (2013) Morphological and biochemical characterization of the membranous hepatitis C virus replication compartment. *J. Virol.* **87**, 10612–10627 [CrossRef Medline](#)
8. Lohmann, V., Körner, F., Herian, U., and Bartenschlager, R. (1997) Biochemical properties of hepatitis C virus NS5B RNA-dependent RNA polymerase and identification of amino acid sequence motifs essential for enzymatic activity. *J. Virol.* **71**, 8416–8428 [Medline](#)
9. Bressanelli, S., Tomei, L., Roussel, A., Incitti, I., Vitale, R. L., Mathieu, M., De Francesco, R., and Rey, F. A. (1999) Crystal structure of the RNA-dependent RNA polymerase of hepatitis C virus. *Proc. Natl. Acad. Sci. U.S.A.* **96**, 13034–13039 [CrossRef Medline](#)
10. Tellinghuisen, T. L., Foss, K. L., Treadaway, J. C., and Rice, C. M. (2008) Identification of residues required for RNA replication in domains II and III of the hepatitis C virus NS5A protein. *J. Virol.* **82**, 1073–1083 [CrossRef Medline](#)
11. Tellinghuisen, T. L., Marcotrigiano, J., and Rice, C. M. (2005) Structure of the zinc-binding domain of an essential component of the hepatitis C virus replicase. *Nature* **435**, 374–379 [CrossRef Medline](#)
12. Appel, N., Zayas, M., Miller, S., Krijnse-Locker, J., Schaller, T., Friebe, P., Kallis, S., Engel, U., and Bartenschlager, R. (2008) Essential role of domain III of nonstructural protein 5A for hepatitis C virus infectious particle assembly. *PLoS Pathog.* **4**, e1000035 [CrossRef Medline](#)
13. Ahn, J., Chung, K.-S., Kim, D.-U., Won, M., Kim, L., Kim, K.-S., Nam, M., Choi, S.-J., Kim, H.-C., Yoon, M., Chae, S.-K., and Hoe, K.-L. (2004) Systematic identification of hepatocellular proteins interacting with NS5A of the hepatitis C virus. *J. Biochem. Mol. Biol.* **37**, 741–748 [Medline](#)
14. de Chassey, B., Navratil, V., Tafforeau, L., Hiet, M. S., Aublin-Gex, A., Agaügué, S., Meiffren, G., Pradezynski, F., Faria, B. F., Chantier, T., Le Breton, M., Pellet, J., Davoust, N., Mangeot, P. E., Chaboud, A., et al. (2008) Hepatitis C virus infection protein network. *Mol. Syst. Biol.* **4**, 230 [Medline](#)
15. Bessa, L. M., Launay, H., Dujardin, M., Cantrelle, F.-X., Lippens, G., Landrieu, I., Schneider, R., and Hanouille, X. (2017) NMR reveals the intrinsically disordered domain 2 of NS5A protein as an allosteric regulator of the hepatitis C virus RNA polymerase NS5B. *J. Biol. Chem.* **292**, 18024–18043 [CrossRef Medline](#)
16. Penin, F., Brass, V., Appel, N., Ramboarina, S., Montserret, R., Ficheux, D., Blum, H. E., Bartenschlager, R., and Moradpour, D. (2004) Structure and function of the membrane anchor domain of hepatitis C virus nonstructural protein 5A. *J. Biol. Chem.* **279**, 40835–40843 [CrossRef Medline](#)
17. Liang, Y., Ye, H., Kang, C. B., and Yoon, H. S. (2007) Domain 2 of nonstructural protein 5A (NS5A) of hepatitis C virus is natively unfolded. *Biochemistry* **46**, 11550–11558 [CrossRef Medline](#)
18. Hanouille, X., Badillo, A., Verdegem, D., Penin, F., and Lippens, G. (2010) The domain 2 of the HCV NS5A protein is intrinsically unstructured. *Protein Pept. Lett.* **17**, 1012–1018 [CrossRef Medline](#)
19. Hanouille, X., Verdegem, D., Badillo, A., Wieruszkeski, J.-M., Penin, F., and Lippens, G. (2009) Domain 3 of non-structural protein 5A from hepatitis C virus is natively unfolded. *Biochem. Biophys. Res. Commun.* **381**, 634–638 [CrossRef Medline](#)
20. Love, R. A., Brodsky, O., Hickey, M. J., Wells, P. A., and Cronin, C. N. (2009) Crystal structure of a novel dimeric form of NS5A domain I protein from hepatitis C virus. *J. Virol.* **83**, 4395–4403 [CrossRef Medline](#)
21. Lambert, S. M., Langley, D. R., Garnett, J. A., Angell, R., Hedgethorpe, K., Meanwell, N. A., and Matthews, S. J. (2014) The crystal structure of NS5A domain 1 from genotype 1a reveals new clues to the mechanism of action for dimeric HCV inhibitors. *Protein Sci.* **23**, 723–734 [CrossRef Medline](#)
22. Huang, L., Hwang, J., Sharma, S. D., Hargittai, M. R., Chen, Y., Arnold, J. J., Raney, K. D., and Cameron, C. E. (2005) Hepatitis C virus nonstructural protein 5A (NS5A) is an RNA-binding protein. *J. Biol. Chem.* **280**, 36417–36428 [CrossRef Medline](#)
23. Gao, M., Nettles, R. E., Belema, M., Snyder, L. B., Nguyen, V. N., Fridell, R. A., Serrano-Wu, M. H., Langley, D. R., Sun, J. H., O'Boyle, D. R., Lemm, J. A., Wang, C., Knipe, J. O., Chien, C., Colonna, R. J., et al. (2010) Chemical genetics strategy identifies an HCV NS5A inhibitor with a potent clinical effect. *Nature* **465**, 96–100 [CrossRef Medline](#)
24. O'Boyle, D. R., Sun, J.-H., Nower, P. T., Lemm, J. A., Fridell, R. A., Wang, C., Romine, J. L., Belema, M., Nguyen, V. N., Laurent, D. R. St, Serrano-Wu, M., Snyder, L. B., Meanwell, N. A., Langley, D. R., and Gao, M. (2013) Characterizations of HCV NS5A replication complex inhibitors. *Virology* **444**, 343–354 [CrossRef Medline](#)
25. Hanouille, X., Badillo, A., Wieruszkeski, J. M., Verdegem, D., Landrieu, I., Bartenschlager, R., Penin, F., and Lippens, G. (2009) Hepatitis C virus NS5A protein is a substrate for the peptidyl-prolyl cis/trans isomerase activity of cyclophilins A and B. *J. Biol. Chem.* **284**, 13589–13601 [CrossRef Medline](#)
26. Verdegem, D., Badillo, A., Wieruszkeski, J.-M., Landrieu, I., Leroy, A., Bartenschlager, R., Penin, F., Lippens, G., and Hanouille, X. (2011) Domain 3 of NS5A protein from the Hepatitis C Virus has intrinsic  $\alpha$ -helical propensity and is a substrate of cyclophilin A. *J. Biol. Chem.* **286**, 20441–20454 [CrossRef Medline](#)
27. Chatterji, U., Lim, P., Bobardt, M. D., Wieland, S., Cordek, D. G., Vuagniaux, G., Chisari, F., Cameron, C. E., Targett-Adams, P., Parkinson, T., and Gallay, P. A. (2010) HCV resistance to cyclosporin A does not correlate with a resistance of the NS5A-cyclophilin A interaction to cyclophilin inhibitors. *J. Hepatol.* **53**, 50–56 [CrossRef Medline](#)
28. Yang, F., Robotham, J. M., Grise, H., Frausto, S., Madan, V., Zayas, M., Bartenschlager, R., Robinson, M., Greenstein, A. E., Nag, A., Logan, T. M., Bienkiewicz, E., and Tang, H. (2010) A major determinant of cyclophilin dependence and cyclosporine susceptibility of hepatitis C virus identified by a genetic approach. *PLoS Pathog.* **6**, e1001118 [CrossRef Medline](#)
29. Grisé, H., Frausto, S., Logan, T., and Tang, H. (2012) A conserved tandem cyclophilin-binding site in hepatitis C virus nonstructural protein 5A regulates Alisporivir susceptibility. *J. Virol.* **86**, 4811–4822 [CrossRef Medline](#)
30. Dujardin, M., Madan, V., Montserret, R., Ahuja, P., Huvent, I., Launay, H., Leroy, A., Bartenschlager, R., Penin, F., Lippens, G., and Hanouille, X. (2015) A proline-tryptophan turn in the intrinsically disordered domain 2 of NS5A protein is essential for hepatitis C virus RNA replication. *J. Biol. Chem.* **290**, 19104–19120 [CrossRef Medline](#)
31. Fernandes, F., Ansari, I. U., and Striker, R. (2010) Cyclosporine inhibits a direct interaction between cyclophilins and hepatitis C NS5A. *PLoS ONE* **5**, e9815 [CrossRef Medline](#)
32. Hopkins, S., Scorneaux, B., Huang, Z., Murray, M. G., Wring, S., Smitley, C., Harris, R., Erdmann, F., Fischer, G., and Ribeill, Y. (2010) SCY-635, a novel nonimmunosuppressive analog of cyclosporine that exhibits potent inhibition of hepatitis C virus RNA replication *in vitro*. *Antimicrob. Agents Chemother.* **54**, 660–672 [CrossRef Medline](#)
33. Ma, S., Boerner, J. E., TiongYip, C., Weidmann, B., Ryder, N. S., Cooreman, M. P., and Lin, K. (2006) NIM811, a cyclophilin inhibitor, exhibits potent *in vitro* activity against hepatitis C virus alone or in combination with  $\alpha$  interferon. *Antimicrob. Agents Chemother.* **50**, 2976–2982 [CrossRef Medline](#)
34. Ahmed-Belkacem, A., Colliandre, L., Ahnou, N., Nevers, Q., Gelin, M., Bessin, Y., Brillet, R., Cala, O., Douguet, D., Bourguet, W., Krimm, I., Pawlotsky, J.-M., and Guichou, J.-F. (2016) Fragment-based discovery of a new family of non-peptidic small-molecule cyclophilin inhibitors with potent antiviral activities. *Nat. Commun.* **7**, 12777 [CrossRef Medline](#)
35. Kaufmann, S. H. E., Dorhoi, A., Hotchkiss, R. S., and Bartenschlager, R. (2018) Host-directed therapies for bacterial and viral infections. *Nat. Rev. Drug Discov.* **17**, 35–56 [CrossRef Medline](#)
36. Yang, F., Robotham, J. M., Nelson, H. B., Irsigler, A., Kenworthy, R., and Tang, H. (2008) Cyclophilin A is an essential cofactor for hepatitis C virus infection and the principal mediator of cyclosporine resistance *in vitro*. *J. Virol.* **82**, 5269–5278 [CrossRef Medline](#)

## Conformational regulation of NS5A-D2 by CypA

37. Chatterji, U., Bobardt, M., Selvarajah, S., Yang, F., Tang, H., Sakamoto, N., Vuagniaux, G., Parkinson, T., and Gallay, P. (2009) The isomerase active site of cyclophilin A is critical for hepatitis C virus replication. *J. Biol. Chem.* **284**, 16998–17005 [CrossRef Medline](#)
38. Madan, V., Paul, D., Lohmann, V., and Bartenschlager, R. (2014) Inhibition of HCV replication by cyclophilin antagonists is linked to replication fitness and occurs by inhibition of membranous web formation. *Gastroenterology* **146**, 1361–1372.e1–9 [CrossRef Medline](#)
39. Chatterji, U., Bobardt, M., Tai, A., Wood, M., and Gallay, P. A. (2015) Cyclophilin and NS5A inhibitors, but not other anti-HCV agents, preclude HCV-mediated formation of double membrane vesicle viral factories. *Antimicrob. Agents Chemother.* **59**, 2496–2507 [CrossRef Medline](#)
40. Chatterji, U., Bobardt, M., Schaffer, L., Wood, M., and Gallay, P. A. (2016) Cyclophilin inhibitors remodel the endoplasmic reticulum of HCV-infected cells in a unique pattern rendering cells impervious to a reinfection. *PLoS ONE* **11**, e0159511 [CrossRef Medline](#)
41. Goto, K., Watashi, K., Inoue, D., Hijikata, M., and Shimotohno, K. (2009) Identification of cellular and viral factors related to anti-hepatitis C virus activity of cyclophilin inhibitor. *Cancer Sci.* **100**, 1943–1950 [CrossRef Medline](#)
42. Nevers, Q., Ruiz, I., Ahnou, N., Donati, F., Brillet, R., Softic, L., Chazal, M., Jouvenet, N., Fourati, S., Baudesson, C., Bruscella, P., Gelin, M., Guichou, J.-F., Pawlotsky, J.-M., and Ahmed-Belkacem, A. (2018) Characterization of the anti-hepatitis C virus activity of new nonpeptidic small-molecule cyclophilin inhibitors with the potential for broad anti-flaviviridae activity. *Antimicrob. Agents Chemother.* **62**, e00126–18 [Medline](#)
43. Garcia-Rivera, J. A., Bobardt, M., Chatterji, U., Hopkins, S., Gregory, M. A., Wilkinson, B., Lin, K., and Gallay, P. A. (2012) Multiple mutations in hepatitis C virus NS5A domain II are required to confer a significant level of resistance to alisporivir. *Antimicrob. Agents Chemother.* **56**, 5113–5121 [CrossRef Medline](#)
44. Coelmont, L., Hanouille, X., Chatterji, U., Berger, C., Snoeck, J., Bobardt, M., Lim, P., Vliegen, I., Paeshuyse, J., Vuagniaux, G., Vandamme, A. M., Bartenschlager, R., Gallay, P., Lippens, G., and Neyts, J. (2010) DEB025 (Alisporivir) inhibits hepatitis C virus replication by preventing a cyclophilin A induced cis-trans isomerisation in domain II of NS5A. *PLoS ONE* **5**, e13687 [CrossRef Medline](#)
45. Tompa, P. (2002) Intrinsically unstructured proteins. *Trends Biochem. Sci.* **27**, 527–533 [CrossRef Medline](#)
46. Uversky, V. N. (2013) A decade and a half of protein intrinsic disorder: biology still waits for physics: protein intrinsic disorder. *Protein Sci.* **22**, 693–724 [CrossRef Medline](#)
47. Borgia, A., Borgia, M. B., Bugge, K., Kissling, V. M., Heidarsson, P. O., Fernandes, C. B., Sottini, A., Soranno, A., Buholzer, K. J., Nettels, D., Kragelund, B. B., Best, R. B., and Schuler, B. (2018) Extreme disorder in an ultrahigh-affinity protein complex. *Nature* **555**, 61–66 [CrossRef Medline](#)
48. Uversky, V. N., Oldfield, C. J., and Dunker, A. K. (2008) Intrinsically disordered proteins in human diseases: introducing the D2 concept. *Annu. Rev. Biophys.* **37**, 215–246 [CrossRef Medline](#)
49. Tompa, P., and Fuxreiter, M. (2008) Fuzzy complexes: polymorphism and structural disorder in protein–protein interactions. *Trends Biochem. Sci.* **33**, 2–8 [CrossRef Medline](#)
50. Gould, C. M., Diella, F., Via, A., Puntervoll, P., Gemünd, C., Chabanis-Davidson, S., Michael, S., Sayadi, A., Bryne, J. C., Chica, C., Seiler, M., Davey, N. E., Haslam, N., Weatheritt, R. J., Budd, A., et al. (2010) ELM: the status of the 2010 eukaryotic linear motif resource. *Nucleic Acids Res.* **38**, D167–D180 [CrossRef Medline](#)
51. Vacic, V., Oldfield, C. J., Mohan, A., Radivojac, P., Cortese, M. S., Uversky, V. N., and Dunker, A. K. (2007) Characterization of molecular recognition features, MoRFs, and their binding partners. *J. Proteome Res.* **6**, 2351–2366 [CrossRef Medline](#)
52. Fuxreiter, M., Simon, I., Friedrich, P., and Tompa, P. (2004) Preformed structural elements feature in partner recognition by intrinsically unstructured proteins. *J. Mol. Biol.* **338**, 1015–1026 [CrossRef Medline](#)
53. Zhou, J., Zhao, S., and Dunker, A. K. (2018) Intrinsically disordered proteins link alternative splicing and post-translational modifications to complex cell signaling and regulation. *J. Mol. Biol.* **430**, 2342–2359 [CrossRef Medline](#)
54. Theillet, F.-X., Kalmar, L., Tompa, P., Han, K.-H., Selenko, P., Dunker, A. K., Daughdrill, G. W., and Uversky, V. N. (2013) The alphabet of intrinsic disorder I: act like a pro: on the abundance and roles of proline residues in intrinsically disordered proteins. *Intrinsically Disord. Proteins* **1**, e24360 [CrossRef Medline](#)
55. Changeux, J.-P. (2013) 50 years of allosteric interactions: the twists and turns of the models. *Nat. Rev. Mol. Cell Biol.* **14**, 819–829 [CrossRef Medline](#)
56. Hilser, V. J., and Thompson, E. B. (2007) Intrinsic disorder as a mechanism to optimize allosteric coupling in proteins. *Proc. Natl. Acad. Sci. U.S.A.* **104**, 8311–8315 [CrossRef Medline](#)
57. Motlagh, H. N., Wrabl, J. O., Li, J., and Hilser, V. J. (2014) The ensemble nature of allostery. *Nature* **508**, 331–339 [CrossRef Medline](#)
58. Bah, A., and Forman-Kay, J. D. (2016) Modulation of intrinsically disordered protein function by post-translational modifications. *J. Biol. Chem.* **291**, 6696–6705 [CrossRef Medline](#)
59. Feuerstein, S., Solyom, Z., Aladag, A., Favier, A., Schwarten, M., Hoffmann, S., Willbold, D., and Brutscher, B. (2012) Transient structure and SH3 interaction sites in an intrinsically disordered fragment of the hepatitis C virus protein NS5A. *J. Mol. Biol.* **420**, 310–323 [CrossRef Medline](#)
60. Tamiola, K., Acar, B., and Mulder, F. A. (2010) Sequence-specific random coil chemical shifts of intrinsically disordered proteins. *J. Am. Chem. Soc.* **132**, 18000–18003 [CrossRef Medline](#)
61. Zondlo, N. J. (2013) Aromatic-proline interactions: electronically tunable CH/π interactions. *Acc. Chem. Res.* **46**, 1039–1049 [CrossRef Medline](#)
62. Chung, H.-Y., Gu, M., Buehler, E., MacDonald, M. R., and Rice, C. M. (2014) Seed sequence-matched controls reveal limitations of small interfering RNA knockdown in functional and structural studies of hepatitis C virus NS5A-MOBKL1B interaction. *J. Virol.* **88**, 11022–11033 [CrossRef Medline](#)
63. Kosol, S., Contreras-Martos, S., Cedeño, C., and Tompa, P. (2013) Structural characterization of intrinsically disordered proteins by NMR spectroscopy. *Molecules* **18**, 10802–10828 [CrossRef Medline](#)
64. Jensen, M. R., Markwick, P. R., Meier, S., Griesinger, C., Zweckstetter, M., Grzesiek, S., Bernadó, P., and Blackledge, M. (2009) Quantitative determination of the conformational properties of partially folded and intrinsically disordered proteins using NMR dipolar couplings. *Structure* **17**, 1169–1185 [CrossRef Medline](#)
65. Ahuja, P., Cantrelle, F.-X., Huvent, I., Hanouille, X., Lopez, J., Smet, C., Wieruszkeski, J.-M., Landrieu, I., and Lippens, G. (2016) Proline conformation in a functional Tau fragment. *J. Mol. Biol.* **428**, 79–91 [CrossRef Medline](#)
66. Farrow, N. A., Zhang, O., Forman-Kay, J. D., and Kay, L. E. (1994) A heteronuclear correlation experiment for simultaneous determination of <sup>15</sup>N longitudinal decay and chemical exchange rates of systems in slow equilibrium. *J. Biomol. NMR* **4**, 727–734 [CrossRef Medline](#)
67. Saleh, T., Jankowski, W., Sriram, G., Rossi, P., Shah, S., Lee, K.-B., Cruz, L. A., Rodriguez, A. J., Birge, R. B., and Kalodimos, C. G. (2016) Cyclophilin A promotes cell migration via the Abl-Crk signaling pathway. *Nat. Chem. Biol.* **12**, 117–123 [CrossRef Medline](#)
68. Stollar, E. J., Lin, H., Davidson, A. R., and Forman-Kay, J. D. (2012) Differential dynamic engagement within 24 SH3 domain: peptide complexes revealed by co-linear chemical shift perturbation analysis. *PLoS ONE* **7**, e51282 [CrossRef Medline](#)
69. Selvaratnam, R., VanSchouwen, B., Fogolari, F., Mazhab-Jafari, M. T., Das, R., and Melacini, G. (2012) The projection analysis of NMR chemical shifts reveals extended EPAC autoinhibition determinants. *Biophys. J.* **102**, 630–639 [CrossRef Medline](#)
70. Selvaratnam, R., Chowdhury, S., VanSchouwen, B., and Melacini, G. (2011) Mapping allostery through the covariance analysis of NMR chemical shifts. *Proc. Natl. Acad. Sci. U.S.A.* **108**, 6133–6138 [CrossRef Medline](#)
71. Mu, Y., Nguyen, P. H., and Stock, G. (2005) Energy landscape of a small peptide revealed by dihedral angle principal component analysis. *Proteins* **58**, 45–52 [Medline](#)
72. Ilizaliturri-Flores, I., Correa-Basurto, J., Bello, M., Rosas-Trigueros, J. L., Zamora-López, B., Benítez-Cardoza, C. G., and Zamorano-Carrillo, A.

- (2016) Mapping the intrinsically disordered properties of the flexible loop domain of Bcl-2: a molecular dynamics simulation study. *J. Mol. Model* **22**, 98 [CrossRef Medline](#)
73. Han, B., Liu, Y., Ginzinger, S. W., and Wishart, D. S. (2011) SHIFTX2: significantly improved protein chemical shift prediction. *J. Biomol. NMR* **50**, 43–57 [CrossRef Medline](#)
74. Egger, D., Wölk, B., Gosert, R., Bianchi, L., Blum, H. E., Moradpour, D., and Bienz, K. (2002) Expression of hepatitis C virus proteins induces distinct membrane alterations including a candidate viral replication complex. *J. Virol.* **76**, 5974–5984 [CrossRef Medline](#)
75. Liu, Z., Yang, F., Robotham, J. M., and Tang, H. (2009) Critical role of cyclophilin A and its prolyl-peptidyl isomerase activity in the structure and function of the hepatitis C virus replication complex. *J. Virol.* **83**, 6554–6565 [CrossRef Medline](#)
76. Fernandes, F., Poole, D. S., Hoover, S., Middleton, R., Andrei, A. C., Gerstner, J., and Striker, R. (2007) Sensitivity of hepatitis C virus to cyclosporine A depends on nonstructural proteins NS5A and NS5B. *Hepatology* **46**, 1026–1033 [CrossRef Medline](#)
77. Liu, C., Perilla, J. R., Ning, J., Lu, M., Hou, G., Ramalho, R., Himes, B. A., Zhao, G., Bedwell, G. J., Byeon, I.-J., Ahn, J., Gronenborn, A. M., Prevelige, P. E., Rousso, I., Aiken, C., et al. (2016) Cyclophilin A stabilizes the HIV-1 capsid through a novel non-canonical binding site. *Nat. Commun.* **7**, 10714 [CrossRef Medline](#)
78. Luban, J., Bossolt, K. L., Franke, E. K., Kalpana, G. V., and Goff, S. P. (1993) Human immunodeficiency virus type 1 Gag protein binds to cyclophilins A and B. *Cell* **73**, 1067–1078 [CrossRef Medline](#)
79. Franke, E. K., Yuan, H. E., and Luban, J. (1994) Specific incorporation of cyclophilin A into HIV-1 virions. *Nature* **372**, 359–362 [CrossRef Medline](#)
80. Thali, M., Bukovsky, A., Kondo, E., Rosenwirth, B., Walsh, C. T., Sodroski, J., and Göttlinger, H. G. (1994) Functional association of cyclophilin A with HIV-1 virions. *Nature* **372**, 363–365 [CrossRef Medline](#)
81. Bosco, D. A., Eisenmesser, E. Z., Pochapsky, S., Sundquist, W. I., and Kern, D. (2002) Catalysis of cis/trans isomerization in native HIV-1 capsid by human cyclophilin A. *Proc. Natl. Acad. Sci. U.S.A.* **99**, 5247–5252 [CrossRef](#)
82. Aberham, C., Weber, S., and Phares, W. (1996) Spontaneous mutations in the human immunodeficiency virus type 1 gag gene that affect viral replication in the presence of cyclosporins. *J. Virol.* **70**, 3536–3544 [Medline](#)
83. Ylinen, L. M., Schaller, T., Price, A., Fletcher, A. J., Noursadeghi, M., James, L. C., and Towers, G. J. (2009) Cyclophilin A levels dictate infection efficiency of human immunodeficiency virus type 1 capsid escape mutants A92E and G94D. *J. Virol.* **83**, 2044–2047 [CrossRef Medline](#)
84. Lu, M., Hou, G., Zhang, H., Suiter, C. L., Ahn, J., Byeon, I.-J., Perilla, J. R., Langmead, C. J., Hung, I., Gor'kov, P. L., Gan, Z., Brey, W., Aiken, C., Zhang, P., Schulten, K., Gronenborn, A. M., and Polenova, T. (2015) Dynamic allostery governs cyclophilin A–HIV capsid interplay. *Proc. Natl. Acad. Sci. U.S.A.* **112**, 14617–14622 [CrossRef Medline](#)
85. Quinn, C. M., Wang, M., Fritz, M. P., Runge, B., Ahn, J., Xu, C., Perilla, J. R., Gronenborn, A. M., and Polenova, T. (2018) Dynamic regulation of HIV-1 capsid interaction with the restriction factor TRIM5 $\alpha$  identified by magic-angle spinning NMR and molecular dynamics simulations. *Proc. Natl. Acad. Sci. U.S.A.* **115**, 11519–11524 [CrossRef Medline](#)
86. Rosnoblet, C., Fritzing, B., Legrand, D., Launay, H., Wieruszski, J.-M., Lippens, G., and Hanouille, X. (2012) Hepatitis C virus NS5B and host cyclophilin A share a common binding site on NS5A. *J. Biol. Chem.* **287**, 44249–44260 [CrossRef Medline](#)
87. Ngure, M., Issur, M., Shkriabai, N., Liu, H.-W., Cosa, G., Kvaratskhelia, M., and Götte, M. (2016) Interactions of the disordered domain II of hepatitis C virus NS5A with cyclophilin A, NS5B, and viral RNA show extensive overlap. *ACS Infect. Dis.* **2**, 839–851 [CrossRef Medline](#)
88. Combet, C., Garnier, N., Charavay, C., Grando, D., Crisan, D., Lopez, J., Dehne-Garcia, A., Geourjon, C., Bettler, E., Hulo, C., Le Mercier, P., Bartenschlager, R., Diepolder, H., Moradpour, D., Pawlotsky, J. M., et al. (2007) euHCVdb: the European hepatitis C virus database. *Nucleic Acids Res.* **35**, D363–6 [CrossRef Medline](#)
89. Combet, C., Blanchet, C., Geourjon, C., and Deléage, G. (2000) NPS@: network protein sequence analysis. *Trends Biochem. Sci.* **25**, 147–150 [CrossRef Medline](#)
90. Lee, W., Tonelli, M., and Markley, J. L. (2015) NMRFAM-SPARKY: enhanced software for biomolecular NMR spectroscopy. *Bioinform. Oxf. Engl.* **31**, 1325–1327 [CrossRef](#)
91. Verdegem, D., Dijkstra, K., Hanouille, X., and Lippens, G. (2008) Graphical interpretation of Boolean operators for protein NMR assignments. *J. Biomol. NMR* **42**, 11–21 [CrossRef Medline](#)
92. Ottiger, M., Delaglio, F., and Bax, A. (1998) Measurement of J and dipolar couplings from simplified two-dimensional NMR spectra. *J. Magn. Reson.* **131**, 373–378 [CrossRef Medline](#)
93. Cornilescu, G., Delaglio, F., and Bax, A. (1999) Protein backbone angle restraints from searching a database for chemical shift and sequence homology. *J. Biomol. NMR* **13**, 289–302 [CrossRef Medline](#)
94. Brunger, A. T., Adams, P. D., Clore, G. M., DeLano, W. L., Gros, P., Grosse-Kunstleve, R. W., Jiang, J. S., Kuszewski, J., Nilges, M., Pannu, N. S., Read, R. J., Rice, L. M., Simonson, T., and Warren, G. L. (1998) Crystallography & NMR system: a new software suite for macromolecular structure determination. *Acta Crystallogr. Biol. Crystallogr.* **54**, 905–921 [CrossRef](#)
95. Schrodinger, LLC. (2015) *The PyMOL Molecular Graphics System*, version 1.8, Schroedinger, LLC, New York
96. Salomon-Ferrer, R., Case, D. A., and Walker, R. C. (2013) An overview of the Amber biomolecular simulation package: Amber biomolecular simulation package. *Wiley Interdiscip. Rev. Comput. Mol. Sci.* **3**, 198–210 [CrossRef](#)
97. Case, D. A., Cheatham, T. E., 3rd, Darden, T., Gohlke, H., Luo, R., Merz, K. M., Jr., Onufriev, A., Simmerling, C., Wang, B., and Woods, R. J. (2005) The Amber biomolecular simulation programs. *J. Comput. Chem.* **26**, 1668–1688 [CrossRef Medline](#)
98. Salomon-Ferrer, R., Götz, A. W., Poole, D., Le Grand, S., and Walker, R. C. (2013) Routine microsecond molecular dynamics simulations with AMBER on GPUs: 2. explicit solvent particle mesh Ewald. *J. Chem. Theory Comput.* **9**, 3878–3888 [CrossRef Medline](#)
99. Hornak, V., Abel, R., Okur, A., Strockbine, B., Roitberg, A., and Simmerling, C. (2006) Comparison of multiple Amber force fields and development of improved protein backbone parameters. *Proteins* **65**, 712–725 [CrossRef](#)
100. Lindorff-Larsen, K., Piana, S., Palmo, K., Maragakis, P., Klepeis, J. L., Dror, R. O., and Shaw, D. E. (2010) Improved side-chain torsion potentials for the Amber ff99SB protein force field. *Proteins* **78**, 1950–1958 [Medline](#)
101. Miao, Y., Feher, V. A., and McCammon, J. A. (2015) Gaussian accelerated molecular dynamics: unconstrained enhanced sampling and free energy calculation. *J. Chem. Theory Comput.* **11**, 3584–3595 [CrossRef Medline](#)

**Cyclophilin A allows the allosteric regulation of a structural motif in the disordered domain 2 of NS5A and thereby fine-tunes HCV RNA replication**  
Marie Dujardin, Vanesa Madan, Neha S. Gandhi, François-Xavier Cantrelle, H  l  ne Launay, Isabelle Huvent, Ralf Bartenschlager, Guy Lippens and Xavier Hanouille

*J. Biol. Chem.* 2019, 294:13171-13185.

doi: 10.1074/jbc.RA119.009537 originally published online July 17, 2019

---

Access the most updated version of this article at doi: [10.1074/jbc.RA119.009537](https://doi.org/10.1074/jbc.RA119.009537)

Alerts:

- [When this article is cited](#)
- [When a correction for this article is posted](#)

[Click here](#) to choose from all of JBC's e-mail alerts

This article cites 100 references, 33 of which can be accessed free at <http://www.jbc.org/content/294/35/13171.full.html#ref-list-1>